Intermittent Cytomegalovirus Infection Alters Neurobiological Metabolism and Induces Cognitive Deficits in Mice

Mark A.A. Harrison[1, 4], Sara L. Morris[2, 4], Grace A. Rudman[3], Daniel J. Rittenhouse[4, 11], Chandler H. Monk[5], Siva SVP Sakamuri[6], MaryJane J. Jones[4], Md Mehedi Hasan[7], Mst Shamima Khatun[11], Hanyun Wang[9], Lucas P. Garfinkel[9], Elizabeth B. Norton[4], Chad Steele[4,8], Sangku Kim[7], Jay K. Kolls[10,11], S. Michal Jazwinski[7,8, 10], Ricardo Mostany[6, 8], Prasad VG Katakam[6, 7, 8], Elizabeth B. Engler-Chiurazzi[8, 9], Kevin J. Zwezdaryk[4, 7, 8]

[1]Neuroscience Program, Tulane Brain Institute, Tulane University School of Science & Engineering, New Orleans, LA 70112, USA
[2]Biomedical Sciences Program, Tulane University School of Medicine, New Orleans, LA 70112, USA
[3]Department of Environmental Studies, Tulane University School of Liberal Arts, New Orleans, LA 70112, USA
[4]Department of Microbiology & Immunology, Tulane University School of Medicine, New Orleans, LA 70112, USA
[5]Bioinnovation Program, Tulane University School of Medicine, New Orleans, LA 70112, USA
[6]Department of Pharmacology, Tulane University School of Medicine, New Orleans, LA 70112, USA
[7]Tulane Center for Aging, Tulane University School of Medicine, New Orleans, LA 70112, USA
[8]Tulane Brain Institute, Tulane University School of Medicine, New Orleans, LA 70112, USA
[9]Department of Neurosurgery, Tulane University School of Medicine, New Orleans, LA 70112, USA
[10]Deming Department of Medicine, Tulane University School of Medicine, New Orleans, LA 70112, USA
[11]Tulane Center for Translational Research in Infection & Inflammation, Tulane University School of Medicine, New Orleans, LA 70112, USA

Correspondence
kzwezdar@tulane.edu (K.J.Z), eenglerchiurazzi@tulane.edu (E.B.EC)

In Brief

Mechanistic evidence supporting an infectious etiology of dementia (e.g. Alzheimer's Disease) are poorly defined. Harrison et al., show that intermittent infection with cytomegalovirus metabolically rewires the blood brain barrier and neighboring glial cells altering their function, resulting in decreased cognitive function.

Keywords

Alzheimer's Disease, cognitive decline, cytomegalovirus, metabolism, oxidative stress, brain microvascular endothelial cells, blood brain barrier, virus, aging, dementia

SUMMARY

Risk factors contributing to dementia are multifactorial. Pathogens as risk factors for dementia is largely correlative with few causal relationships. Here, we demonstrate that intermittent cytomegalovirus (CMV) infection in mice, mimicking human chronic infection and reactivation/reinfection events, alters blood brain barrier (BBB) metabolic pathways. An increase in basal mitochondrial function is observed in brain microvasculature endothelial cells (BMEC) at 12 months post infection but not at earlier time points and is accompanied by elevated levels of superoxide, indicative of oxidative stress. Further, these mice score lower in cognitive assays as compared to age-matched controls. Our data show that repeated systemic infection with CMV, alters BBB metabolic function and impacts cognition. These observations provide mechanistic insights through which pathogens contribute to the progression of pathologies associated with dementia.

INTRODUCTION

Aging is a primary risk factor associated with cognitive decline and the development of dementia, such as Alzheimer's disease (AD) (Hou et al., 2019; Moir et al., 2018). Therapeutic strategies have focused on extracellular amyloid-beta (Aβ) oligomers and soluble fragments, or intracellular hyperphosphorylated-tau tangles. However, these hallmarks of AD are not evident until the disease has been developing for years and, even at that point, patients are often in a pre-clinical phase of the disease with little to no cognitive symptoms (Dubois et al., 2016; Guzman-Velez et al., 2022). These findings suggest that other initiating or contributing factors exist which may be addressed decades prior to the development of any cognitive symptoms.

Pathogens are increasingly recognized as risk factors in the etiology of age-associated neurodegeneration (Harris and Harris, 2015; Moir et al., 2018). A single viral or bacterial infection in adult rodents has been shown to promote sickness behavior, induce systemic and central nervous system (CNS) inflammatory cascades, alter memory performance, and disrupted synaptic communication via neuronal

63 loss (Hritcu et al., 2011; Kahn et al., 2012; Kranjac et al., 2012; McLinden et al., 2012; Tarr et al., 2011;
64 Zhao et al., 2019). Humans do not experience a single infection during their lifetimes, but rather
65 intermittent infections throughout life. The long-term consequences of intermittent infection are
66 inadequately studied. Emerging preclinical evidence suggests that a higher lifetime infection burden
67 impairs cognition, especially among transgenic mice carrying AD risk factors (Batista et al., 2019; Harris
68 and Harris, 2015). Finally, studies in adult and aged humans show that higher cumulative exposure to HSV-
69 1, cytomegalovirus (CMV), and bacterial infections was associated with impaired cognitive performance
70 or an accelerated rate of cognitive decline (Dickerson et al., 2014; Katan et al., 2013; Lovheim et al., 2018;
71 Lurain et al., 2013). Converging evidence indicates that pathogen exposure can promote features of
72 dementia but the mechanisms for these effects have yet to be elucidated.

73 In this study, CMV was used a as a model pathogen. CMV is a ubiquitous herpesvirus exhibiting
74 40-80% seropositivity in the human population (Hoehl et al., 2020). Common to all herpesviruses,
75 following acute infection, CMV becomes latent and reactivates sporadically throughout the lifetime of the
76 host resulting in intermittent infection. Further, different CMV strains are thought to infect individuals
77 throughout life. CMV's ability to evade immune clearance enables a persistent phenotype that is
78 associated with immunosenescence, inflammaging, and memory T cell inflation (Holtappels et al., 2000).
79 Most individuals seroconvert before the age of 40 suggesting that the cycle of latency/reactivation or
80 reinfection continues for decades (Bate et al., 2010).

81 The role of CMV in unhealthy aging, including dementias, remains largely correlative. Data
82 suggesting individuals positive for CMV have an increased risk for AD and accelerated cognitive decline
83 (Barnes et al., 2015; Lee et al., 2020) are contrasted with data suggesting a weak association (Warren-
84 Gash et al., 2019). Ultimately, a lack of mechanisms linking pathogens and the origins of dementia impede
85 progress. Intriguingly, CMV pathogenesis mirrors many of the features of AD pathology including calcium
86 dysregulation (Sharon-Friling et al., 2006), amyloid deposition (Lurain et al., 2013), iron dysfunction

(Crowe et al., 2004), autophagic (Taisne et al., 2019), and mitochondrial dysfunction (Betsinger et al., 2021; Combs et al., 2020; Harrison et al., 2022).

The ability of CMV to alter the metabolic profile of host cells to produce the biomaterials and energy needed for viral replication is well described (Combs et al., 2020; Harrison et al., 2022; Saffran et al., 2007; Spaggiari et al., 2008; Suliman et al., 2004; Vastag et al., 2011). This metabolic reprogramming often results in impaired bioenergetics and subsequent increases in reactive oxygen species (ROS) production. Interestingly, ROS production and impaired metabolism have been implicated in numerous neurodegenerative diseases (Cai et al., 2012; Kim et al., 2015; Li et al., 2013; Muddapu et al., 2020). Additionally, the Mitochondrial Cascade Hypothesis posits that AD pathogenesis is driven by progressive mitochondrial dysfunction (Ashleigh et al., 2022). Further, it has been shown that mitochondrial function directly alters the secretion or storage of Aβ (Wilkins et al., 2022). Finally, studies have demonstrated that metabolic and mitochondrial changes alter cellular proteostasis and precede the onset of clinical symptoms of AD (Swerdlow, 2020). Therefore, CMV, with its potent capacity to reprogram cellular metabolism is an ideal candidate for assessing the impact of pathogens on aging-associated pathology such as AD.

In this study, we demonstrate that intermittent CMV infection induces metabolic alterations in the blood brain barrier (BBB) that correlate with decreases in cognitive function. We observe that endothelial cells isolated from the BBB display enhanced oxidative phosphorylation (OXPHOS) and consequently produce elevated levels of superoxide (SO) following the pro-inflammatory immune response. These findings suggest that infection frequency and burden may accelerate cognitive decline by modulating BBB metabolism and increasing oxidative stress.

RESULTS

Intermittent MCMV infection exhibits delayed inflammatory cytokine expression in the brain

Pathogen exposure and burden increase with age (Kline and Bowdish, 2016). Using a reductionist model, we examined how a single herpesvirus (CMV) can contribute to accelerated hallmarks of aging and dementia. As CMV exhibits species tropism, we used the well described Smith strain of murine CMV (MCMV) in our studies(Fisher and Lloyd, 2020). We employed a murine model that integrates intermittent infection and natural aging starting with young adult mice aged 8 weeks (Figure 1A). In immunocompetent individuals, human CMV infection is asymptomatic, or results in mild flu-like symptoms and general malaise. Our murine model behaves similarly, exhibiting slight but significant changes in body weight 2-3 days post infection (DPI), but rapid recovery equaling mock-infected mice by 5 DPI (Figure 1B). Repeat MCMV exposures at 3-, 6-, and 9-months post infection (MPI) do not result in significant changes in body weight (Figure S1A). Additionally, there were no significant changes in weight at 1 MPI (Figure 1C) and mice exposed to intermittent infection did not exhibit significant changes in weight loss over 12 months (Figure S1B). Plasma IgM specific to MCMV exhibited high concentrations 7 DPI after initial infection (Figure 1D) but were reduced by 1 MPI. Subsequently, MCMV specific IgM concentrations increased with reinfection. MCMV specific IgG concentrations correlated strongly with MCMV specific IgM plasma concentration and significantly increased as a function of challenge number and remained quantitively similar from 6-12 MPI (Figure 1E). All mock-infected mice failed to elicit an antibody response against MCMV, confirming the infection status remained negative throughout our experimental timeline. To validate our measured results were not the result of active viral shedding, PCR analysis was completed using salivary glands. MCMV can be detected at high viral loads in the salivary gland (Campbell et al., 2008). At 7 DPI we observed high levels of UL123, a viral gene expressed early during replication. Expression of UL123 decreases by 1 MPI (Figure S1C). There was no replicating MCMV detected in salivary glands at 6- or 12-month timepoints suggesting a functional immune response and establishment of MCMV latency.

Previous reports have suggested that in MCMV models, pro-inflammatory cytokine responses may inhibit the innate immune response contributing to viral pathogenesis (Stacey et al., 2017; Stacey et al., 2011). We observe differential expression of cytokines in relation to infection frequency, time, and the origin of the sample (Figure 1F). In blood at 7 DPI, we observed significant upregulation of pro-and anti-inflammatory cytokines including IL-1β, IL-6, TNFα, IL-12p40, IL-12p70, CCL5, and IL-10 as compared to mock infected animals. (Figure 1G, Figure S1D). CCL5 has previously been identified as a commonly increased chemokine following CMV infection (Caldeira-Dantas et al., 2018; Wang et al., 2004). In contrast, at 7 DPI, we observed mild pro-inflammatory cytokine increases in brain homogenate that was limited to IL-12(p40) and CCL-5 (Figure 1H, Figure S1E). Interestingly, at 1 MPI, we observed an elevated expression of inflammatory cytokines similar to that measured in the periphery at 7 DPI (Figure 1H, Figure S1E). At this timepoint, the inflammation in the periphery was resolved (Figure S1F). However, at 12 MPI, after 4 MCMV challenges, inflammatory cytokine levels in the brain are consistently lower in expression (Figure 1H, Figure S1E) compared to the mock infected controls. This pattern of cytokine expression was not observed in mock-infected mice (Figure S1G). Based on these findings, we conclude that peripheral inflammation results in a delayed inflammatory response in the CNS.

Intermittent MCMV infection alters the transcriptional profile of brain cells

We next used Multiome analysis (simultaneous single cell gene expression and ATAC-seq) to examine transcriptional changes in various cell populations. Whole brain lysate from mock-infected 12 MPI animals was compared to 12 MPI animals that had experienced intermittent CMV infection. Dimensionality reduction analysis using UMAP showed clustering of 7 distinct cell populations based on single-cell RNA expression (Figure 2A), single-cell chromatin accessibility (Figure 2B) and integrated scATAC/scRNA (Figure 2C). To confirm observations from single cell transcriptional data, we assessed brain cells phenotypically and metabolically using spectral flow cytometry (Table S1, Figure S2A). At all

timepoints examined, there were minor changes in the percent of brain cell populations (Figure 2E, 2F, 2G). We observed significant increases in T-cell populations in infected mice at all time points, indicating enhanced extravasation from the bloodstream into the neural parenchyma. Of the other cell types assayed, there were no significant changes between Mock and MCMV infected animals at any timepoint. However in young adult mice, at 7 DPI, we observed increased proliferation rates in activated microglia/macrophages and T cells (Figure 2H). These were accompanied by decreased proliferation of brain microvascular endothelial cells (BMECs) (Figure 2H). Taken together, these findings demonstrate expanding immune populations in response to initial infection or the subsequent inflammatory response. T-cell populations exhibited changes in proliferation rate, as measured by Ki-67 positivity, with a decrease at 1 MPI and an increase at 12 MPI respectively (Figure 2I, 2J).

Blood brain barrier metabolic pathways are altered with increased MCMV exposure

Our current data does not suggest that MCMV in our model directly infects the brain. Others have reported similar findings (Reuter et al., 2004). If peripheral MCMV infection can influence changes in the brain, the initial site of interaction is likely the BBB. Our Multiome data showed significant changes in transcriptional expression of brain endothelial cells associated with metabolism (Slc1a3 and Atp1a2) and BBB function (Cdh5, Cldn5, plpp3, Pla2g7, and Pecm1) (Figure 2D). Due to these findings, we focused on characterizing the metabolic profile of BMECs. We used glucose transporter 1 (GLUT1), hexokinase 2 (HKII), translocase of the outer mitochondrial membrane 20 (TOMM20) and voltage dependent anion channel 1 (VDAC1) as proxies for glycolytic and OXPHOS pathways (Figure 3A). In our characterization of BMECs we identified a large population that had high expression of eNOS while a minority exhibited low eNOS expression. Interestingly, in MCMV infected animals at 7 DPI, both total and eNOS low BMECs had elevated expression of GLUT1 relative to mock infected animals (Figure 3B). This is contrasted with a downregulation of GLUT1 in total BMECs (Figure 3C) and downregulation in the eNOS high group at late

timepoints, as compared to the mock infected controls (Figure 3D). Hexokinase expression at 7 DPI was unchanged (Figure S3A), decreased at 1 MPI (Figure S3B), and only increased at 12 MPI in the eNOS low group (Figure S3C). Taken together, initial infection appears to enhance glycolytic function, but that change is transient and trends towards decreased glycolysis as a function of repeat infection and age. In contrast, mitochondrial pathways trended towards enhancement in young adult mice at 7 DPI as indicated by VDAC1 (Figure 3E) and TOMM20 (Figure S3D) expression. At 1 MPI VDAC1 expression (Figure 3F) is decreased and TOMM20 (Figure S3E) remains unchanged. By 12 MPI, total BMECs and the eNOS high group have significantly upregulated VDAC1 expression which suggests increased OXPHOS function as VDAC1 is the primary channel for ATP/ADP exchange in mitochondria (Figure 3G). Expression of the protein transporter TOMM20 was upregulated in eNOS high groups at 7 DPI (Figure S3D), unchanged at 1 MPI (Figure S3E), and downregulated at 12 MPI (Figure S3F). Previous research has demonstrated that, despite having access to sufficient oxygen, BMECs are highly glycolytic (McDonald et al., 2022). The young adult mice, at 7 DPI, protein expression results suggest that MCMV enhances this metabolic preference. However in aged mice, by 12 MPI, these cells have been reprogrammed to enhance OXPHOS as indicated by VDAC1 protein expression. The impact of these changes is unknown but they suggest altered BMEC metabolic function and possibly BBB integrity.

Hallmarks of mitochondrial dysfunction and oxidative stress are elevated in BMECs intermittently exposed to MCMV

To better understand the impact of altered expression of metabolic markers, we isolated BMECs from the BBB and completed Seahorse bioanalyzer analysis (Figure 4A). At 1 MPI there were no significant changes to OXPHOS including mitochondrial basal respiration, proton leak, non-mitochondrial respiration or mitochondrial ATP production rate (Figure 4B, 4C). Similarly, there were no changes in maximal respiration, spare respiratory capacity or total ATP production rate between mock and infected mice

(Figure S4A). Intriguingly in the aged mice, 12 MPI, the basal respiration rate, the minimal work required by the mitochondria to meet metabolic demand, was significantly increased in MCMV-infected mice (Figure 4D, 4E). This suggests that BMEC mitochondria from infected mice work harder to attain the same level of metabolic homeostasis as BMECs from mock-infected mice. No changes in maximal respiration or spare capacity (Figure S4B) were observed. Critically, we measured significant increases in proton leak and non-mitochondrial respiration (Figure 4E) in BMEC from MCMV infected mice, suggesting the presence of oxidative and mitochondrial stress. Mitochondrial ATP production rate was not found to be increased (Figure 4E). To validate our findings, live cell examination of mitochondria was performed by flow cytometry on $CD31^{+}$ cells isolated from the brain. No changes in mitochondrial mass were detected at 1 MPI (Figure 4F) but increases were observed in aged mice, 12 MPI (Figure 4G), when comparing mock- vs MCMV-infected. Critically, mitochondria-specific superoxide was significantly upregulated only in mice exposed to intermittent infection (Figure 4H, Figure 4I). Together, these data suggest intermittent MCMV infection decreases BMEC mitochondrial efficiency and increases oxidative stress.

MCMV infection metabolically rewires astrocytes as a function of age

We next asked if metabolic changes were restricted to the BBB or if additional changes were occurring in the brain parenchyma. Due to their close interactions and functional cooperation with the BBB, astrocytes were further examined. In addition to total astrocytes we also further subdivided this group into their pro-inflammatory (A1) and anti-inflammatory (A2) phenotypes. Astrocytes uptake metabolites and proteins from the BBB to supply nutrients to neurons (Figure 5A). Global decreases in astrocytic metabolic function, both glycolysis and OXPHOS, have been associated with AD and result in insufficient metabolic support for neighboring neurons (Andersen et al., 2022). GLUT1 in astrocytes is responsible for uptake of glucose from the bloodstream (Zlokovic, 2011) and AD patients have lower glucose levels in the brain (Herholz et al., 2002; Marcus et al., 2014; Mosconi et al., 2010). In young adult

mice, 7 DPI and 1 MPI, GLUT1 expression in astrocytes is unchanged between mock and MCMV-infected mice but decreases in aged mice, 12 MPI (Figure 5B). HKII levels are significantly decreased at 1 MPI but are unchanged at 12 MPI (Figure S5A).

OXPHOS function, as indicated by the protein import channel subunit TOMM20, demonstrated a significant decrease in expression at 12 MPI in the MCMV-infected mice. TOMM20 expression is unchanged in A1 astrocytes at 7 DPI but increases in A2 astrocytes (Figure S5B). However, in aged mice, 12 MPI, total astrocytes showed decreased TOMM20 expression (Figure 5C), findings that repeated in A1 and A2 populations (Figure S5C). These findings suggest that mitochondrial function is altered due to infection burden. No changes in VDAC1 were observed (Figure S5D). Mitochondrial mass did not change at 7 DPI in ACSA-2 positive cells but there was significantly less superoxide production in MCMV-infected animals (Figure 5D). At 1 MPI both mass and superoxide production were similar in both groups of animals (Figure 5E). By 12 MPI the mitochondrial mass of astrocytes in the MCMV-infected mice was significantly decreased, however they were producing similar levels of superoxide (Figure 5F). These findings agree with the decreases in TOMM20; however the similar levels of superoxide suggest increased oxidative stress. Our results suggest that different cell populations in the brain, exhibit distinct metabolic changes in response to intermittent CMV infection and age.

Increased T cell accumulation in the brain

An increased percent of live T cells was detected in both young adult, 7 DPI and 1 MPI, and aged mice, 12 MPI, indicating increased extravasation from the vasculature (Figure 2E, 2F, 2G, 6A, and 6B). In the 1 MPI cohort, T cells had decreased expression of OXPHOS and glycolysis metabolic markers relative to mock infected animals (Figure 6A). In the 12 MPI cohort, T cells had higher expression of OXPHOS and glycolysis metabolic markers relative to mock infected animals (Figure 6B). Additionally, these cells had significantly decreased H3K27me3 expression suggesting a more transcriptionally active population. The

highly bioenergetic nature of these cells and retention in the parenchyma despite the absence of active infection or inflammation suggest that they represent a population of tissue resident T memory cells. Previous literature using a similar MCMV model described brain resident memory CD8 T cells acting as inhibitors of MCMV reactivation (Brizic et al., 2018). The presence of resident memory T cells in the CNS may contribute to disease progression as the CNS has conventionally been perceived as an immune privileged environment.

Cognition is impaired with intermittent MCMV infection

To understand the physical manifestations of our collective molecular results, we completed cognitive assays on all mice used in the experiments described in this manuscript. Hot plate (Figure S6A) and passive avoidance (Figure S6D) assays were completed to identify innate differences in nociceptive ability and fear-aggravated learning. At 1- (Figure S6B) and 12 MPI (Figure S6C), both groups exhibit similar latency to behavior and number of behaviors demonstrating that their nociceptive capabilities are intact and similar between groups (Woolfe and Macdonald, 1944). At 1- (Figure S6E) and 12 MPI (Figure S6F), both groups exhibit near perfect retention of learning after 24 hours. This is indicative that fear-based learning events (shock) with high salience are still able to be learned regardless of infection status. In young adult mice, 7 DPI, Y-maze spontaneous alternation assessment of short-term recognition memory (Figure 6C) demonstrated very similar number of alternations and spontaneous, correct alternations (Figure 6D). At 1 MPI, MCMV-infected mice exhibited a significantly lower number of total alternations, but no significant changes to spontaneous alternations (Figure 6E). Interestingly, in aged mice, 12 MPI (3 months after last infection), no difference in total alternations was measured but there was a significant decrease in spontaneous alternations, indicative of impaired spatial working memory (Figure 6F).

Additionally, we observed a trend towards decreased spontaneous alternations when comparing young adult, 1 MPI, and aged, 12 MPI, mock-infected mice (Figure 6G). These findings are in agreement

279 with previous studies of cognitive impairment in BALB/cJ mice in which cognitive decline was first
280 measurable at 12 months of age (Esquivel et al., 2020). We see a significant decrease in cognition with
281 infection status and age when comparing 1 MPI mock and 12 MPI MCMV-infected cohorts. Collectively,
282 our results suggest that increased viral burden, metabolically reprograms BMEC and glial metabolism,
283 driving BBB dysfunction, T cell infiltration and cognitive decline (Figure 6H). This suggests synergy between
284 viral burden and age as they relate to cognitive decline.
285
286 **DISCUSSION**
287 Dementia, including AD, are identified clinically, years to decades after initiation and progression
288 of disease. Pathogens and the resulting immune response have been correlated to AD but mechanistic
289 evidence integrating an infection and aging is lacking. Here, we addressed the impact of viral infection on
290 several aspects of AD pathology as a function of age. The data demonstrate that intermittent CMV
291 infection exacerbates age-associated mitochondrial dysfunction and oxidative stress. First, repeated
292 MCMV infection increased basal mitochondrial function over time. Second, mitochondrial specific ROS
293 was elevated in aged, repeated MCMV exposed mice. Third, intermittent infection resulted in significant
294 cognitive impairment. Importantly, the intermittently infected mice, even at the latest timepoint, appear
295 and behave just like the mock infected animals.
296 We report that intermittent CMV challenge impacts the metabolic function of endothelial cells in
297 the BBB. The degree of functional change increases with viral burden and age. How these changes are
298 mediated continue to be investigated. Metabolic pathways in BMECs are not altered during primary acute
299 infection in young adult mice. Instead, reprogramming occurs incrementally with increased viral burden
300 in advanced age. Inflammatory cytokines have been strongly associated with changes to BBB permeability
301 (Yang et al., 2019). We observed increased inflammatory markers in the blood at 7 DPI, but only minor
302 changes in the brain (Figure 1). In brain lysate, IL-12p40 was significantly increased correlating with

303 published data showing that siRNA knock-down of IL-12p40 in SAMP8 mice ameliorated AD
304 neuropathology (Tan et al., 2014). IL-12(p40) antagonizes IL-12 function and upregulation is needed for
305 efficient MCMV clearance (Carr et al., 1999). CCL5 was also significantly increased and aids in migration
306 of MCMV-specific $CD8^+$ T cells (Caldeira-Dantas et al., 2018). CMV encodes a highly specific RANTES decoy
307 receptor (Wang et al., 2004) illustrating the importance of this cytokine during CMV infection. Both
308 cytokines continue to be significantly upregulated 1 MPI, possibly due to paracrine effects of low-level
309 viral persistence or residual viral products. Interestingly, both have been linked to Alzheimer's disease
310 (Vacinova et al., 2021; Vom Berg et al., 2012). At 1 MPI, we detect low levels of MCMV replication in the
311 salivary gland (Figure 1). IL-1β and TNFα have been implicated in MCMV reactivation *in vivo* (Cook et al.,
312 2006; Simon et al., 2005) possibly establishing a cycle of intermittent reactivation. We did not include
313 assays to quantify MCMV reactivation in this study design, but the significant increase in IgM levels at the
314 6- and 12-MPI timepoints suggest that MCMV may reactivate more in these cohorts. It has been reported
315 that CMV reactivates more frequently as a function of increased age (Hemmersbach-Miller et al., 2020).
316 Inefficient control of MCMV reactivation by the immune system may explain the emergence of subtle but
317 significant changes at 12 MPI. Surprisingly, cytokine concentrations in the brain are significantly decreased
318 in MCMV infected mice at 12 MPI. Mice were last exposed to MCMV 3 months prior to testing of cytokines
319 so we expected concentrations similar to mock conditions, but not lower concentrations. It is possible
320 that hypoactivation is driving low levels, suggesting dysfunction in one or more glial populations.
321 Alternatively, this may be a response to the delayed expression of inflammatory cytokines seen at 1 MPI.
322 It is also possible that anti-inflammatory mechanisms are over stimulated. Collectively, all scenarios
323 suggest dysregulation of cytokine-associated mechanisms in the brain.

324 Our -omics approach concurs strongly with the molecular changes we observe. In endothelial cells
325 we measure significant transcriptional changes related to BBB permeability and function. Cadherin-5
326 (Cdn5), claudin-5 (Cldn5), and CD31 (Pecam1) are crucial for maintaining tight junction integrity and

permeability (Ma et al., 2017; Wimmer et al., 2019). Increased expression of CD31 has been linked to neuroinflammation and accumulation of leukocytes (Wimmer et al., 2019). Phospholipid phosphatase 3 (Plpp3) and phospholipase A2 (Pla2g7) are associated with vascular maintenance. Interestingly, phospholipase A2 has recently been shown to regulate phospholipid catabolism during inflammatory and oxidative stress responses (Li et al., 2021; Lv et al., 2021; Spadaro et al., 2022). Decreased expression correlated with lower levels of pro-inflammatory cytokines. The sodium-potassium transporter (ATP1A2) and amino acid transporter (Slc1a3) expression changes support the hypothesis of altered metabolic pathways in brain endothelial cells from MCMV infected mice.

The BBB is the interface between the brain and the periphery and includes BMECs, astrocytes, and pericytes that actively regulate the movement of proteins, nutrients, ions, and small molecules. Systemic inflammation could exert effects on the BBB by affecting the BMECs. Our metabolic profiling of BMECs indicated a significant initial increase in GLUT1 expression in MCMV infected animals which is consistent with previous findings where CMV has been reported to upregulate glycolysis pathways during infection (Combs et al., 2020; Harrison et al., 2022; Munger et al., 2006; Yu et al., 2011). Similar upregulation of glycolysis pathways has been reported in AD brains (Mooradian et al., 1997). However, we noted a significant decrease in GLUT1 expression at 12 MPI. This is an area of active exploration in our lab. GLUT1 is the main mediator of glucose uptake for the brain and alterations have been shown to initiate BBB changes, altering tight junction integrity (Winkler et al., 2015). Reduced GLUT1 may be indicative of reprogrammed BMEC metabolism, shifting dependency to OXPHOS which explains increased basal respiration in 12 MPI mice. This would be similar to a recent report showing CRISPR-Cas9 GLUT1 truncation decreased BMEC bioenergetics and negatively impacted neuro angiogenesis (Pervaiz et al., 2022). Expression of claudin-5, the dominant tight junction protein in the BBB, has been shown to decrease in parallel with GLUT1 following suppression of the Wnt/β-catenin pathway (Wang et al., 2022).

Our previous research has demonstrated that CMV infection dysregulates this pathway (Angelova et al., 2012; Zwezdaryk et al., 2016) providing a possible mechanism for these changes.

In addition to the glycolytic changes discussed above, mitochondrial function is significantly altered in MCMV infected BMECs in aged mice, 12 MPI. Our group previously published that CMV infection induces mitochondrial dysfunction in fibroblasts and glioblastoma cell lines (Combs et al., 2020; Harrison et al., 2022). Our current and previous findings are consistent with literature associating metabolism and mitochondrial dysfunction with dementia (Gao et al., 2020; Wilkins and Swerdlow, 2021). VDAC1, the primary channel for the exchange of ADP for ATP through the mitochondrial membrane is intrinsically linked to both the metabolic and the apoptotic functions of mitochondria. The increases in VDAC1 expression and mitochondrial mass with age and infection suggest increased dependence on OXPHOS. Our Seahorse data demonstrate minimal change to mitochondrial ATP production implying OXPHOS is being used for non-bioenergetic purposes. Intriguingly, VDAC1 has been reported to be elevated in the brains of AD patients and in APP transgenic mice (Cuadrado-Tejedor et al., 2011; Manczak and Reddy, 2012). In the context of AD, VDAC1 is required for Aß uptake and apoptosis (Smilansky et al., 2015). Our VDAC1 observations may coincide with hexokinase-influenced glycolytic changes mediating BBB activity (Pastorino et al., 2005). Our model correlates strongly with these studies and demonstrate that further studies exploring VDAC1 function in our model are warranted. Decreased TOMM20 expression was also observed. TOMM20 is responsible for the import of proteins targeted to the mitochondria. A Parkinson's Disease model provided evidence that overexpression of TOMM20 protected against α-synuclein-induced mitochondrial dysfunction and subsequent neurodegeneration (De Miranda et al., 2020). Based on these observations, decreased TOMM20 levels in our model may suggest impaired Aß clearance due to dysfunctional mitochondrial transport functions.

Age and senescence related decreases in glycolysis and OXPHOS have previously been reported in BMECs suggesting that MCMV infection may accelerate an aging phenotype relative to mock infected

374 animals (Sakamuri et al., 2022). Uncoupling of the ETC may explain the increased proton leak and play a
375 protective role by mitigating ROS production and therefore oxidative damage (Divakaruni and Brand,
376 2011). Previous research has shown that increased ROS production in the absence of increased ATP
377 production leads to endothelial cell activation and recruitment of immune cells which is supported by our
378 results (Li et al., 2017). Most intriguing is the detection of increased mitochondrial specific superoxide
379 (Figure 4). ROS has been well documented to contribute to neurodegenerative disorders (Valko et al.,
380 2007) specifically neuronal death due to Aß accumulation (Zhang et al., 2009). We measured an increase
381 in total mitochondria suggesting mitochondrial fission is occurring. This is likely due to metabolic stress
382 and can be induced by CMV infection (Combs et al., 2019; Norris and Youle, 2008). It would be interesting
383 to define the impact on mitophagy to understand if damaged mitochondria remaining in the BBB further
384 contribute to BBB functional changes and progression of AD related pathologies.

385 Astrocytes, the abundant glial cells that reinforce the BMEC tight junctions in the BBB, act as the
386 primary nutrient uptake agents for the brain. Similar to BMECs, astrocytes expressed significantly
387 decreased levels of GLUT1 at 12 MPI. Astrocytic glycolysis is essential for neuron health as glycolysis-
388 derived lactate is taken up by neurons and used in OXPHOS in axon terminals. Studies have demonstrated
389 that astrocytic glycolysis decreases with age and is thought to contribute to AD-related impairments (Yao
390 et al., 2011). Additionally, astrocytic lactate is critical for providing neurons with the energy needed to
391 function properly and form memories (Descalzi et al., 2019). The impact of reduced glucose supply across
392 the BBB into the cerebral parenchyma was not investigated in our model but may play a critical role linking
393 metabolic rewiring to cognitive changes via reduced nutrient availability to neurons. Measuring glucose
394 and lactate concentrations in cortical and hippocampal regions may provide key insights linking
395 intermittent infection with cognitive decline in our model.

396 The increased presence of T cells in the brain with intermittent infection and age is largely
397 unexplained with our approach but could be driven by increased ROS. We do not detect chronic

inflammation in the periphery or the brain. A leaky BBB would provide increased and easier access for T cells to cross the BBB and these changes correlate with infection, but this alone does not fully explain our results. The highly metabolic nature of these T cells (Figure 6) suggest that they may be tissue resident T cells. Murine polyomavirus infection has been reported to produce a set of brain resident memory T cells (Shwetank et al., 2017). Similar results were observed in Vesicular stomatitis virus (VSV) treated mice and it is thought that their persistence in the CNS may be problematic in an environment unaccustomed to immune surveillance (Wakim et al., 2010). However, these viruses are neurotropic and CMV has significant difficulty crossing the BBB in mature immunocompetent mice (Reuter et al., 2004). Future studies will assess BBB permeability in this model.

The most compelling results linking our molecular results with a physical outcome are our cognitive function behavior tests. Foot-shock based passive avoidance test results were very similar between animals at all timepoints indicating the ability to learn fear-based, high salience stimuli effectively. An aging study in BALB/C mice only found significant differences in passive avoidance cognition beginning at 24 months of age (Puglisi-Allegra et al., 1986), so our findings at 12 months were expected. We employed the Y-maze as a measure of spontaneous alternation. Successful alternations between arms indicate an intact short-term recognition memory and by extension suggest intact medial pre-frontal cortex and hippocampal functions. At 1 MPI MCMV-infected mice trend towards a decreased percent of correct alternations in the maze, possible due to lingering sickness behavior (Figure 6) or resulting from the impact of increased pro-inflammatory cytokines in the brain (Figure 1). These events cannot explain the cognitive decline observed at 12 MPI as there is a decreased concentration of pro-inflammatory cytokines (Figure 1). Similarly, age-related activity can be disregarded as both mock and MCMV-infected animals exhibited similar number of alternations in the same timeframe and cognitive performance is determined as a function of total movement in the maze. The significant decrease in cognitive function when merging the cofactors age and infection strongly points to a synergy between

CMV infection and age. A study in BALB/c mice was first able to detect cognitive decline using the Y-maze when comparing 4 month old mice to 12 month old mice (Esquivel et al., 2020). The fact that we detected impaired cognition with age matched controls at the 12 MPI timepoint strongly suggests that MCMV infection accelerates cognitive decline.

CMV seropositivity has previously been associated with numerous pathologies including breast and brain cancers (Cobbs et al., 2002; Cui et al., 2018; Harkins et al., 2010), suggesting it may play an oncomodulatory role in disease development and/or progression. Anti-viral therapy targeting CMV has been used to treat patients with glioblastoma and has been shown to increase both overall and progression-free survival (Stragliotto et al., 2020a; Stragliotto et al., 2020b). We have demonstrated that systemic inflammation produces a delayed neuroinflammatory response which may be an initiation event for accelerated cognitive decline. We have linked these changes to altered metabolism in BMECs and enhanced production of ROS suggesting mitochondrial dysfunction and oxidative stress may be driving accelerated disease progression. MCMV is our model pathogen, however, any pathogen, including SARS-CoV-2, which produces transient systemic inflammation, may have the potential to contribute to accelerated cellular aging. It is the additive nature of these pathogen exposures over time which we suspect synergize with myriad other factors to accelerate aging and disease pathology.

Our experimental design includes limitations. We attempted a reductionist approach in which our animals were repeatedly exposed to a single pathogen, very dissimilar to the diverse pathogens experienced throughout life. We also employed a mouse model which is phenotypically “normal” with respect to many of the risk factors strongly correlated with the development of dementia or AD. Our goal was to determine if repeated infection, mimicking the intermittent reactivation or reinfection of CMV that occurs throughout life, without any other complicating factors, could recapitulate some aspects of an AD phenotype. Further, it is unknown, and likely variable, how frequently CMV reactivates in an immunocompetent individual. Our model assumes a single reactivation each decade. For this study,

prioritized assessment of structures and processes governing the brain-immune interface so we did not measure Aβ plaques or accumulation of tau tangles, hallmarks of AD. This study also used female mice only, future studies will include males to compare results from current models of dementia and aging (Esquivel et al., 2020). Many of our assays used whole brain or a hemisphere. Despite the generation of exciting data, a region-specific analysis would be of great benefit to further understand how intermittent infection is impacting specific areas of the BBB. Applying this model to transgenic animals predisposed to AD development would provide additional insight into specific cell populations or molecular pathways that change over time. These are all approaches currently being considered by our team.

In summary, our data demonstrate that intermittent CMV infection alters metabolic pathways in the BBB and accelerates cognitive decline. This model makes use of a genotypically and phenotypically normal mouse strain with no predisposition to cognitive deficits or dementia pathology. At 14 months of age, the mice are equivalent to a human in their forties, at which point a human developing dementia would still be in the pro-dromal, symptomless phase. Similar to the course of human disease, MCMV-infected mice are clinically indistinguishable from the controls. Thus our model demonstrates synergy between infection burden and age as potential contributing factors in AD progression. Our work strongly supports a role for pathogens as risk factors in dementia related pathologies. These findings may change the way that we address pathogen exposure and infections especially in populations at a higher risk of developing of dementia.

AKNOWLEDGEMENTS

The authors would like to thank Constance Porretta of the Flow Cytometry Shared Resource Lab for her assistance in developing and running the multiplexed spectral flow panel. We also would like to thank Robin Kamucheka for her help using De Novo's FCS Express 7 for our flow analysis and Dr. Raul Freitas, Ms. India Pursell and Ms. Miayla Marcus for technical input. Finally, we would like to thank Dr. Kejing Song

from the NextGen Sequencing Core for processing our Multiome samples and the Genomics, Bioinformatics, and Spatial Multiomics Core for help with data analysis.

M.A.A.H was supported by a Louisiana Board of Regents predoctoral fellowship (LEQSF 2017-22-GF-11). P.V.K & R.M. are supported by grants from the NIH, 1R01AG074489 (NIA) and 1R01NS114286 (NINDS). R.M is supported by 1R56AG072676. J.K.K was supported by the Louisiana Board of Regents Endowed Chairs for Eminent Scholars program and PHS grant R35HL139930. E.B.EC is supported by K01MH117343. S.M.J is supported by NIGMS P30GM145498. S.M.J and K.J.Z are supported by NIGMS (P20GM103629). K.J.Z and E.B.EC are supported by pilot grants from the Infectious Disease Society of America (IDSA) and the Tulane Brain Institute.

AUTHOR CONTRIBUTIONS

Conceptualization, M.A.A.H., E.B.EC., and K.J.Z.; Methodology, M.A.A.H. and K.J.Z.; Formal Analysis, M.A.A.H., M.J.J., M.M.H. M.S.K., and S.K., K.J.Z.; Investigation, M.A.A.H., S.L.M., G.A.R., D.J.R., C.H.M., S.SVP.S., H.W., L.P.G, M.J.J., and E.B.EC.; Resources, K.J.Z., E.B.N., C.S., and J.K.K.; Data Curation, M.A.A.H. and K.J.Z.; Writing, M.A.A.H. and K.J.Z.; Review and Editing, S.L.M., S.SVP.S., S.K., J.K.K., S.M.J., R.M., and E.B.EC; Visualization, M.A.A.H., M.M.H., M.S.K., S.K., E.B.EC, K.J.Z; Supervision, K.J.Z., S.K., R.M., and P.K.; Project Administration, K.J.Z.; Funding Acquisition K.J.Z. and S.M.J.

DECLARATION OF INTERESTS

The authors declare no competing interests.

REFERENCES

Andersen, J.V., Schousboe, A., and Verkhratsky, A. (2022). Astrocyte energy and neurotransmitter metabolism in Alzheimer's disease: Integration of the glutamate/GABA-glutamine cycle. Prog Neurobiol *217*, 102331.

Angelova, M., Zwezdaryk, K., Ferris, M., Shan, B., Morris, C.A., and Sullivan, D.E. (2012). Human cytomegalovirus infection dysregulates the canonical Wnt/beta-catenin signaling pathway. PLoS Pathog *8*, e1002959.

Ashleigh, T., Swerdlow, R.H., and Beal, M.F. (2022). The role of mitochondrial dysfunction in Alzheimer's disease pathogenesis. Alzheimers Dement.

Barnes, L.L., Capuano, A.W., Aiello, A.E., Turner, A.D., Yolken, R.H., Torrey, E.F., and Bennett, D.A. (2015). Cytomegalovirus infection and risk of Alzheimer disease in older black and white individuals. J Infect Dis *211*, 230-237.

Bate, S.L., Dollard, S.C., and Cannon, M.J. (2010). Cytomegalovirus seroprevalence in the United States: the national health and nutrition examination surveys, 1988-2004. Clin Infect Dis *50*, 1439-1447.

Batista, C.R.A., Gomes, G.F., Candelario-Jalil, E., Fiebich, B.L., and de Oliveira, A.C.P. (2019). Lipopolysaccharide-Induced Neuroinflammation as a Bridge to Understand Neurodegeneration. Int J Mol Sci *20*.

Betsinger, C.N., Jankowski, C.S.R., Hofstadter, W.A., Federspiel, J.D., Otter, C.J., Jean Beltran, P.M., and Cristea, I.M. (2021). The human cytomegalovirus protein pUL13 targets mitochondrial cristae architecture to increase cellular respiration during infection. Proc Natl Acad Sci U S A *118*, 1-12.

Brizic, I., Susak, B., Arapovic, M., Huszthy, P.C., Hirsl, L., Kvestak, D., Juranic Lisnic, V., Golemac, M., Pernjak Pugel, E., Tomac, J.*, et al.* (2018). Brain-resident memory CD8(+) T cells induced by congenital CMV infection prevent brain pathology and virus reactivation. Eur J Immunol *48*, 950-964.

Cai, H., Cong, W.N., Ji, S., Rothman, S., Maudsley, S., and Martin, B. (2012). Metabolic dysfunction in Alzheimer's disease and related neurodegenerative disorders. Curr Alzheimer Res *9*, 5-17.

Caldeira-Dantas, S., Furmanak, T., Smith, C., Quinn, M., Teos, L.Y., Ertel, A., Kurup, D., Tandon, M., Alevizos, I., and Snyder, C.M. (2018). The Chemokine Receptor CXCR3 Promotes CD8(+) T Cell Accumulation in Uninfected Salivary Glands but Is Not Necessary after Murine Cytomegalovirus Infection. J Immunol *200*, 1133-1145.

Campbell, A.E., Cavanaugh, V.J., and Slater, J.S. (2008). The salivary glands as a privileged site of cytomegalovirus immune evasion and persistence. Med Microbiol Immunol *197*, 205-213.

Carr, J.A., Rogerson, J.A., Mulqueen, M.J., Roberts, N.A., and Nash, A.A. (1999). The role of endogenous interleukin-12 in resistance to murine cytomegalovirus (MCMV) infection and a novel action for endogenous IL-12 p40. J Interferon Cytokine Res *19*, 1145-1152.

525 Cobbs, C.S., Harkins, L., Samanta, M., Gillespie, G.Y., Bharara, S., King, P.H., Nabors, L.B., Cobbs, C.G., and
526 Britt, W.J. (2002). Human cytomegalovirus infection and expression in human malignant glioma. Cancer
527 Res *62*, 3347-3350.
528 Combs, J.A., Norton, E.B., Saifudeen, Z.R., Bentrup, K.H.Z., Katakam, P.V., Morris, C.A., Myers, L., Kaur, A.,
529 Sullivan, D.E., and Zwezdaryk, K.J. (2020). Human Cytomegalovirus Alters Host Cell Mitochondrial Function
530 during Acute Infection. J Virol *94*, 1-19.
531 Combs, J.A., Norton, E.B., Saifudeen, Z.R., Honer Zu Bentrup, K., Katakam, P.V., Morris, C.A., Myers, L.,
532 Kaur, A., Sullivan, D.E., and Zwezdaryk, K.J. (2019). Human Cytomegalovirus Alters Host Cell Mitochondrial
533 Function During Acute Infection. J Virol.
534 Cook, C.H., Trgovcich, J., Zimmerman, P.D., Zhang, Y., and Sedmak, D.D. (2006). Lipopolysaccharide, tumor
535 necrosis factor alpha, or interleukin-1beta triggers reactivation of latent cytomegalovirus in
536 immunocompetent mice. J Virol *80*, 9151-9158.
537 Crowe, W.E., Maglova, L.M., Ponka, P., and Russell, J.M. (2004). Human cytomegalovirus-induced host cell
538 enlargement is iron dependent. Am J Physiol Cell Physiol *287*, C1023-1030.
539 Cuadrado-Tejedor, M., Vilarino, M., Cabodevilla, F., Del Rio, J., Frechilla, D., and Perez-Mediavilla, A.
540 (2011). Enhanced expression of the voltage-dependent anion channel 1 (VDAC1) in Alzheimer's disease
541 transgenic mice: an insight into the pathogenic effects of amyloid-beta. J Alzheimers Dis *23*, 195-206.
542 Cui, J., Wang, Q., Wang, H.B., Wang, B., and Li, L. (2018). Protein and DNA evidences of HCMV infection in
543 primary breast cancer tissues and metastatic sentinel lymph nodes. Cancer Biomark *21*, 769-780.
544 De Miranda, B.R., Rocha, E.M., Castro, S.L., and Greenamyre, J.T. (2020). Protection from alpha-Synuclein
545 induced dopaminergic neurodegeneration by overexpression of the mitochondrial import receptor
546 TOM20. NPJ Parkinsons Dis *6*, 38.
547 Descalzi, G., Gao, V., Steinman, M.Q., Suzuki, A., and Alberini, C.M. (2019). Lactate from astrocytes fuels
548 learning-induced mRNA translation in excitatory and inhibitory neurons. Commun Biol *2*, 247.
549 Dickerson, F., Stallings, C., Origoni, A., Katsafanas, E., Schweinfurth, L.A., Savage, C.L., and Yolken, R.
550 (2014). Association between cytomegalovirus antibody levels and cognitive functioning in non-elderly
551 adults. PLoS One *9*, e95510.
552 Divakaruni, A.S., and Brand, M.D. (2011). The regulation and physiology of mitochondrial proton leak.
553 Physiology (Bethesda) *26*, 192-205.
554 Dubois, B., Hampel, H., Feldman, H.H., Scheltens, P., Aisen, P., Andrieu, S., Bakardjian, H., Benali, H.,
555 Bertram, L., Blennow, K.*, et al.* (2016). Preclinical Alzheimer's disease: Definition, natural history, and
556 diagnostic criteria. Alzheimers Dement *12*, 292-323.

Esquivel, N., Garcia, Y., Lores, B., Gutierrez, M., and Rodriguez, C. (2020). Characterization of aged male BALB/ccenp mice as a model of dementia. Lab Anim Res *36*, 7.

Fisher, M.A., and Lloyd, M.L. (2020). A Review of Murine Cytomegalovirus as a Model for Human Cytomegalovirus Disease-Do Mice Lie? International journal of molecular sciences *22*.

Gao, F., Zuo, B., Wang, Y., Li, S., Yang, J., and Sun, D. (2020). Protective function of exosomes from adipose tissue-derived mesenchymal stem cells in acute kidney injury through SIRT1 pathway. Life Sci *255*, 117719.

Guzman-Velez, E., Diez, I., Schoemaker, D., Pardilla-Delgado, E., Vila-Castelar, C., Fox-Fuller, J.T., Baena, A., Sperling, R.A., Johnson, K.A., Lopera, F.*, et al.* (2022). Amyloid-beta and tau pathologies relate to distinctive brain dysconnectomics in preclinical autosomal-dominant Alzheimer's disease. Proc Natl Acad Sci U S A *119*, e2113641119.

Harkins, L.E., Matlaf, L.A., Soroceanu, L., Klemm, K., Britt, W.J., Wang, W., Bland, K.I., and Cobbs, C.S. (2010). Detection of human cytomegalovirus in normal and neoplastic breast epithelium. Herpesviridae *1*, 8.

Harris, S.A., and Harris, E.A. (2015). Herpes Simplex Virus Type 1 and Other Pathogens are Key Causative Factors in Sporadic Alzheimer's Disease. J Alzheimers Dis *48*, 319-353.

Harrison, M.A.A., Hochreiner, E.M., Benjamin, B.P., Lawler, S.E., and Zwezdaryk, K.J. (2022). Metabolic Reprogramming of Glioblastoma Cells during HCMV Infection Induces Secretome-Mediated Paracrine Effects in the Microenvironment. Viruses *14*.

Hemmersbach-Miller, M., Alexander, B.D., Pieper, C.F., and Schmader, K.E. (2020). Age matters: older age as a risk factor for CMV reactivation in the CMV serostatus-positive kidney transplant recipient. Eur J Clin Microbiol Infect Dis *39*, 455-463.

Herholz, K., Salmon, E., Perani, D., Baron, J.C., Holthoff, V., Frolich, L., Schonknecht, P., Ito, K., Mielke, R., Kalbe, E.*, et al.* (2002). Discrimination between Alzheimer dementia and controls by automated analysis of multicenter FDG PET. Neuroimage *17*, 302-316.

Hoehl, S., Berger, A., Ciesek, S., and Rabenau, H.F. (2020). Thirty years of CMV seroprevalence-a longitudinal analysis in a German university hospital. Eur J Clin Microbiol Infect Dis *39*, 1095-1102.

Holtappels, R., Pahl-Seibert, M.F., Thomas, D., and Reddehase, M.J. (2000). Enrichment of immediate-early 1 (m123/pp89) peptide-specific CD8 T cells in a pulmonary CD62L(lo) memory-effector cell pool during latent murine cytomegalovirus infection of the lungs. J Virol *74*, 11495-11503.

Hou, Y., Dan, X., Babbar, M., Wei, Y., Hasselbalch, S.G., Croteau, D.L., and Bohr, V.A. (2019). Ageing as a risk factor for neurodegenerative disease. Nat Rev Neurol *15*, 565-581.

588 Hritcu, L., Ciobica, A., Stefan, M., Mihasan, M., Palamiuc, L., and Nabeshima, T. (2011). Spatial memory
589 deficits and oxidative stress damage following exposure to lipopolysaccharide in a rodent model of
590 Parkinson's disease. Neurosci Res *71*, 35-43.
591 Kahn, M.S., Kranjac, D., Alonzo, C.A., Haase, J.H., Cedillos, R.O., McLinden, K.A., Boehm, G.W., and
592 Chumley, M.J. (2012). Prolonged elevation in hippocampal Abeta and cognitive deficits following repeated
593 endotoxin exposure in the mouse. Behav Brain Res *229*, 176-184.
594 Katan, M., Moon, Y.P., Paik, M.C., Sacco, R.L., Wright, C.B., and Elkind, M.S. (2013). Infectious burden and
595 cognitive function: the Northern Manhattan Study. Neurology *80*, 1209-1215.
596 Kim, G.H., Kim, J.E., Rhie, S.J., and Yoon, S. (2015). The Role of Oxidative Stress in Neurodegenerative
597 Diseases. Exp Neurobiol *24*, 325-340.
598 Kline, K.A., and Bowdish, D.M. (2016). Infection in an aging population. Curr Opin Microbiol *29*, 63-67.
599 Kranjac, D., McLinden, K.A., Deodati, L.E., Papini, M.R., Chumley, M.J., and Boehm, G.W. (2012). Peripheral
600 bacterial endotoxin administration triggers both memory consolidation and reconsolidation deficits in
601 mice. Brain Behav Immun *26*, 109-121.
602 Lee, K.H., Kwon, D.E., Do Han, K., La, Y., and Han, S.H. (2020). Association between cytomegalovirus end-
603 organ diseases and moderate-to-severe dementia: a population-based cohort study. BMC Neurol *20*, 216.
604 Li, J., O, W., Li, W., Jiang, Z.G., and Ghanbari, H.A. (2013). Oxidative stress and neurodegenerative
605 disorders. Int J Mol Sci *14*, 24438-24475.
606 Li, Q., Feng, C., Li, L., Xu, G., Gu, H., Li, S., Li, D., Liu, M., Han, S., and Zheng, B. (2021). Lipid Receptor G2A-
607 Mediated Signal Pathway Plays a Critical Role in Inflammatory Response by Promoting Classical
608 Macrophage Activation. J Immunol *206*, 2338-2352.
609 Li, X., Fang, P., Yang, W.Y., Chan, K., Lavallee, M., Xu, K., Gao, T., Wang, H., and Yang, X. (2017).
610 Mitochondrial ROS, uncoupled from ATP synthesis, determine endothelial activation for both
611 physiological recruitment of patrolling cells and pathological recruitment of inflammatory cells. Can J
612 Physiol Pharmacol *95*, 247-252.
613 Lovheim, H., Olsson, J., Weidung, B., Johansson, A., Eriksson, S., Hallmans, G., and Elgh, F. (2018).
614 Interaction between Cytomegalovirus and Herpes Simplex Virus Type 1 Associated with the Risk of
615 Alzheimer's Disease Development. J Alzheimers Dis *61*, 939-945.
616 Lurain, N.S., Hanson, B.A., Martinson, J., Leurgans, S.E., Landay, A.L., Bennett, D.A., and Schneider, J.A.
617 (2013). Virological and immunological characteristics of human cytomegalovirus infection associated with
618 Alzheimer disease. J Infect Dis *208*, 564-572.

619 Lv, S.L., Zeng, Z.F., Gan, W.Q., Wang, W.Q., Li, T.G., Hou, Y.F., Yan, Z., Zhang, R.X., and Yang, M. (2021). Lp-
620 PLA2 inhibition prevents Ang II-induced cardiac inflammation and fibrosis by blocking macrophage NLRP3
621 inflammasome activation. Acta Pharmacol Sin *42*, 2016-2032.
622 Ma, S.C., Li, Q., Peng, J.Y., Zhouwen, J.L., Diao, J.F., Niu, J.X., Wang, X., Guan, X.D., Jia, W., and Jiang, W.G.
623 (2017). Claudin-5 regulates blood-brain barrier permeability by modifying brain microvascular endothelial
624 cell proliferation, migration, and adhesion to prevent lung cancer metastasis. CNS Neurosci Ther *23*, 947-
625 960.
626 Manczak, M., and Reddy, P.H. (2012). Abnormal interaction of VDAC1 with amyloid beta and
627 phosphorylated tau causes mitochondrial dysfunction in Alzheimer's disease. Hum Mol Genet *21*, 5131-
628 5146.
629 Marcus, C., Mena, E., and Subramaniam, R.M. (2014). Brain PET in the diagnosis of Alzheimer's disease.
630 Clin Nucl Med *39*, e413-422; quiz e423-416.
631 McDonald, C.J., Blankenheim, Z.J., and Drewes, L.R. (2022). Brain Endothelial Cells: Metabolic Flux and
632 Energy Metabolism. Handb Exp Pharmacol *273*, 59-79.
633 McLinden, K.A., Kranjac, D., Deodati, L.E., Kahn, M., Chumley, M.J., and Boehm, G.W. (2012). Age
634 exacerbates sickness behavior following exposure to a viral mimetic. Physiol Behav *105*, 1219-1225.
635 Moir, R.D., Lathe, R., and Tanzi, R.E. (2018). The antimicrobial protection hypothesis of Alzheimer's
636 disease. Alzheimers Dement *14*, 1602-1614.
637 Mooradian, A.D., Chung, H.C., and Shah, G.N. (1997). GLUT-1 expression in the cerebra of patients with
638 Alzheimer's disease. Neurobiol Aging *18*, 469-474.
639 Mosconi, L., Berti, V., Glodzik, L., Pupi, A., De Santi, S., and de Leon, M.J. (2010). Pre-clinical detection of
640 Alzheimer's disease using FDG-PET, with or without amyloid imaging. J Alzheimers Dis *20*, 843-854.
641 Muddapu, V.R., Dharshini, S.A.P., Chakravarthy, V.S., and Gromiha, M.M. (2020). Neurodegenerative
642 Diseases - Is Metabolic Deficiency the Root Cause? Front Neurosci *14*, 213.
643 Munger, J., Bajad, S.U., Coller, H.A., Shenk, T., and Rabinowitz, J.D. (2006). Dynamics of the cellular
644 metabolome during human cytomegalovirus infection. PLoS Pathog *2*, e132.
645 Norris, K.L., and Youle, R.J. (2008). Cytomegalovirus proteins vMIA and m38.5 link mitochondrial
646 morphogenesis to Bcl-2 family proteins. J Virol *82*, 6232-6243.
647 Pastorino, J.G., Hoek, J.B., and Shulga, N. (2005). Activation of glycogen synthase kinase 3beta disrupts
648 the binding of hexokinase II to mitochondria by phosphorylating voltage-dependent anion channel and
649 potentiates chemotherapy-induced cytotoxicity. Cancer Res *65*, 10545-10554.

650 Pervaiz, I., Zahra, F.T., Mikelis, C.M., and Al-Ahmad, A.J. (2022). An in vitro model of glucose transporter 1
651 deficiency syndrome at the blood-brain barrier using induced pluripotent stem cells. J Neurochem *162*,
652 483-500.
653 Puglisi-Allegra, S., Cabib, S., Ebel, A., Kempf, J., and Castellano, C. (1986). Passive avoidance behavior in
654 mice: interaction between age and genotype. Exp Aging Res *12*, 107-109.
655 Reuter, J.D., Gomez, D.L., Wilson, J.H., and Van Den Pol, A.N. (2004). Systemic immune deficiency
656 necessary for cytomegalovirus invasion of the mature brain. J Virol *78*, 1473-1487.
657 Saffran, H.A., Pare, J.M., Corcoran, J.A., Weller, S.K., and Smiley, J.R. (2007). Herpes simplex virus
658 eliminates host mitochondrial DNA. EMBO Rep *8*, 188-193.
659 Sakamuri, S., Sure, V.N., Kolli, L., Liu, N., Evans, W.R., Sperling, J.A., Busija, D.W., Wang, X., Lindsey, S.H.,
660 Murfee, W.L.*, et al.* (2022). Glycolytic and Oxidative Phosphorylation Defects Precede the Development
661 of Senescence in Primary Human Brain Microvascular Endothelial Cells. Geroscience *44*, 1975-1994.
662 Sharon-Friling, R., Goodhouse, J., Colberg-Poley, A.M., and Shenk, T. (2006). Human cytomegalovirus
663 pUL37x1 induces the release of endoplasmic reticulum calcium stores. Proc Natl Acad Sci U S A *103*, 19117-
664 19122.
665 Shwetank, Abdelsamed, H.A., Frost, E.L., Schmitz, H.M., Mockus, T.E., Youngblood, B.A., and Lukacher,
666 A.E. (2017). Maintenance of PD-1 on brain-resident memory CD8 T cells is antigen independent. Immunol
667 Cell Biol *95*, 953-959.
668 Simon, C.O., Seckert, C.K., Dreis, D., Reddehase, M.J., and Grzimek, N.K. (2005). Role for tumor necrosis
669 factor alpha in murine cytomegalovirus transcriptional reactivation in latently infected lungs. J Virol *79*,
670 326-340.
671 Smilansky, A., Dangoor, L., Nakdimon, I., Ben-Hail, D., Mizrachi, D., and Shoshan-Barmatz, V. (2015). The
672 Voltage-dependent Anion Channel 1 Mediates Amyloid beta Toxicity and Represents a Potential Target
673 for Alzheimer Disease Therapy. J Biol Chem *290*, 30670-30683.
674 Spadaro, O., Youm, Y., Shchukina, I., Ryu, S., Sidorov, S., Ravussin, A., Nguyen, K., Aladyeva, E., Predeus,
675 A.N., Smith, S.R.*, et al.* (2022). Caloric restriction in humans reveals immunometabolic regulators of health
676 span. Science *375*, 671-677.
677 Spaggiari, G.M., Capobianco, A., Abdelrazik, H., Becchetti, F., Mingari, M.C., and Moretta, L. (2008).
678 Mesenchymal stem cells inhibit natural killer-cell proliferation, cytotoxicity, and cytokine production: role
679 of indoleamine 2,3-dioxygenase and prostaglandin E2. Blood *111*, 1327-1333.

Stacey, M.A., Clare, S., Clement, M., Marsden, M., Abdul-Karim, J., Kane, L., Harcourt, K., Brandt, C., Fielding, C.A., Smith, S.E*., et al.* (2017). The antiviral restriction factor IFN-induced transmembrane protein 3 prevents cytokine-driven CMV pathogenesis. J Clin Invest *127*, 1463-1474.

Stacey, M.A., Marsden, M., Wang, E.C., Wilkinson, G.W., and Humphreys, I.R. (2011). IL-10 restricts activation-induced death of NK cells during acute murine cytomegalovirus infection. J Immunol *187*, 2944-2952.

Stragliotto, G., Pantalone, M.R., Rahbar, A., Bartek, J., and Soderberg-Naucler, C. (2020a). Valganciclovir as Add-on to Standard Therapy in Glioblastoma Patients. Clin Cancer Res *26*, 4031-4039.

Stragliotto, G., Pantalone, M.R., Rahbar, A., and Soderberg-Naucler, C. (2020b). Valganciclovir as Add-On to Standard Therapy in Secondary Glioblastoma. Microorganisms *8*.

Suliman, H.B., Welty-Wolf, K.E., Carraway, M., Tatro, L., and Piantadosi, C.A. (2004). Lipopolysaccharide induces oxidative cardiac mitochondrial damage and biogenesis. Cardiovasc Res *64*, 279-288.

Swerdlow, R.H. (2020). The mitochondrial hypothesis: Dysfunction, bioenergetic defects, and the metabolic link to Alzheimer's disease. Int Rev Neurobiol *154*, 207-233.

Taisne, C., Lussignol, M., Hernandez, E., Moris, A., Mouna, L., and Esclatine, A. (2019). Human cytomegalovirus hijacks the autophagic machinery and LC3 homologs in order to optimize cytoplasmic envelopment of mature infectious particles. Sci Rep *9*, 4560.

Tan, M.S., Yu, J.T., Jiang, T., Zhu, X.C., Guan, H.S., and Tan, L. (2014). IL12/23 p40 inhibition ameliorates Alzheimer's disease-associated neuropathology and spatial memory in SAMP8 mice. J Alzheimers Dis *38*, 633-646.

Tarr, A.J., McLinden, K.A., Kranjac, D., Kohman, R.A., Amaral, W., and Boehm, G.W. (2011). The effects of age on lipopolysaccharide-induced cognitive deficits and interleukin-1beta expression. Behav Brain Res *217*, 481-485.

Vacinova, G., Vejrazkova, D., Rusina, R., Holmerova, I., Vankova, H., Jarolimova, E., Vcelak, J., Bendlova, B., and Vankova, M. (2021). Regulated upon activation, normal T cell expressed and secreted (RANTES) levels in the peripheral blood of patients with Alzheimer's disease. Neural Regen Res *16*, 796-800.

Valko, M., Leibfritz, D., Moncol, J., Cronin, M.T., Mazur, M., and Telser, J. (2007). Free radicals and antioxidants in normal physiological functions and human disease. Int J Biochem Cell Biol *39*, 44-84.

Vastag, L., Koyuncu, E., Grady, S.L., Shenk, T.E., and Rabinowitz, J.D. (2011). Divergent effects of human cytomegalovirus and herpes simplex virus-1 on cellular metabolism. PLoS Pathog *7*, e1002124.

Vom Berg, J., Prokop, S., Miller, K.R., Obst, J., Kalin, R.E., Lopategui-Cabezas, I., Wegner, A., Mair, F., Schipke, C.G., Peters, O.*, et al.* (2012). Inhibition of IL-12/IL-23 signaling reduces Alzheimer's disease-like pathology and cognitive decline. Nat Med *18*, 1812-1819.

Wakim, L.M., Woodward-Davis, A., and Bevan, M.J. (2010). Memory T cells persisting within the brain after local infection show functional adaptations to their tissue of residence. Proc Natl Acad Sci U S A *107*, 17872-17879.

Wang, D., Bresnahan, W., and Shenk, T. (2004). Human cytomegalovirus encodes a highly specific RANTES decoy receptor. Proc Natl Acad Sci U S A *101*, 16642-16647.

Wang, Q., Huang, X., Su, Y., Yin, G., Wang, S., Yu, B., Li, H., Qi, J., Chen, H., Zeng, W.*, et al.* (2022). Activation of Wnt/beta-catenin pathway mitigates blood-brain barrier dysfunction in Alzheimer's disease. Brain.

Warren-Gash, C., Forbes, H.J., Williamson, E., Breuer, J., Hayward, A.C., Mavrodaris, A., Ridha, B.H., Rossor, M.N., Thomas, S.L., and Smeeth, L. (2019). Human herpesvirus infections and dementia or mild cognitive impairment: a systematic review and meta-analysis. Sci Rep *9*, 4743.

Wilkins, H.M., and Swerdlow, R.H. (2021). Mitochondrial links between brain aging and Alzheimer's disease. Transl Neurodegener *10*, 33.

Wilkins, H.M., Troutwine, B.R., Menta, B.W., Manley, S.J., Strope, T.A., Lysaker, C.R., and Swerdlow, R.H. (2022). Mitochondrial Membrane Potential Influences Amyloid-beta Protein Precursor Localization and Amyloid-beta Secretion. J Alzheimers Dis *85*, 381-394.

Wimmer, I., Tietz, S., Nishihara, H., Deutsch, U., Sallusto, F., Gosselet, F., Lyck, R., Muller, W.A., Lassmann, H., and Engelhardt, B. (2019). PECAM-1 Stabilizes Blood-Brain Barrier Integrity and Favors Paracellular T-Cell Diapedesis Across the Blood-Brain Barrier During Neuroinflammation. Front Immunol *10*, 711.

Winkler, E.A., Nishida, Y., Sagare, A.P., Rege, S.V., Bell, R.D., Perlmutter, D., Sengillo, J.D., Hillman, S., Kong, P., Nelson, A.R.*, et al.* (2015). GLUT1 reductions exacerbate Alzheimer's disease vasculo-neuronal dysfunction and degeneration. Nat Neurosci *18*, 521-530.

Woolfe, G., and Macdonald, A.D. (1944). THE EVALUATION OF THE ANALGESIC ACTION OF PETHIDINE HYDROCHLORIDE (DEMEROL). Journal of Pharmacology and Experimental Therapeutics *80*, 300.

Yang, C., Hawkins, K.E., Dore, S., and Candelario-Jalil, E. (2019). Neuroinflammatory mechanisms of blood-brain barrier damage in ischemic stroke. Am J Physiol Cell Physiol *316*, C135-C153.

Yao, J., Rettberg, J.R., Klosinski, L.P., Cadenas, E., and Brinton, R.D. (2011). Shift in brain metabolism in late onset Alzheimer's disease: implications for biomarkers and therapeutic interventions. Mol Aspects Med *32*, 247-257.

741 Yu, Y., Maguire, T.G., and Alwine, J.C. (2011). Human cytomegalovirus activates glucose transporter 4
742 expression to increase glucose uptake during infection. J Virol *85*, 1573-1580.
743 Zhang, X.D., Wang, Y., Wu, J.C., Lin, F., Han, R., Han, F., Fukunaga, K., and Qin, Z.H. (2009). Down-regulation
744 of Bcl-2 enhances autophagy activation and cell death induced by mitochondrial dysfunction in rat
745 striatum. J Neurosci Res *87*, 3600-3610.
746 Zhao, J., Bi, W., Xiao, S., Lan, X., Cheng, X., Zhang, J., Lu, D., Wei, W., Wang, Y., Li, H.*, et al.* (2019).
747 Neuroinflammation induced by lipopolysaccharide causes cognitive impairment in mice. Sci Rep *9*, 5790.
748 Zlokovic, B.V. (2011). Neurovascular pathways to neurodegeneration in Alzheimer's disease and other
749 disorders. Nat Rev Neurosci *12*, 723-738.
750 Zwezdaryk, K.J., Combs, J.A., Morris, C.A., and Sullivan, D.E. (2016). Regulation of Wnt/beta-catenin
751 signaling by herpesviruses. World J Virol *5*, 144-154.

752

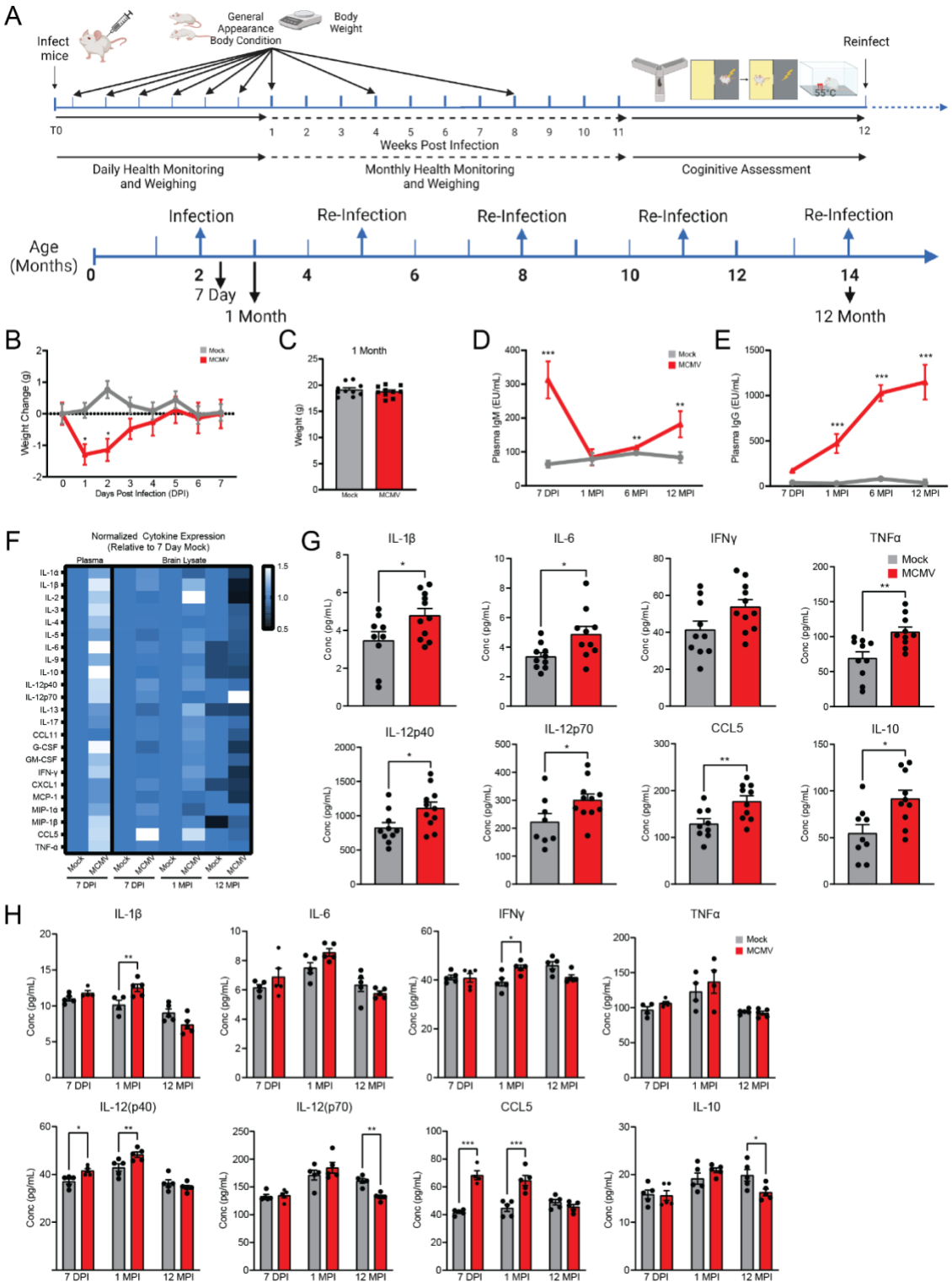

Figure 1: Intermittent MCMV infection exhibits delayed inflammatory cytokine expression in the brain. (A) Schematic outlining the experimental design and re-infection timeline. (B) Weight change in mice over 1 week following initial infection. (C) Weight of mock- (grey) and MCMV-infected (red) mice at 1 month post infection. ELISA-derived concentration of MCMV-specific (D) IgM and (E) IgG from plasma across time. (F) Heatmap of cytokine expression in plasma and brain homogenate at 7 DPI, 1 MPI, and 12 MPI normalized to 7 DPI mock infected measurements. Levels of IL-1β, IL-6, interferon IFNγ, TNFα, IL-12p40, IL12-p70, CCL5, and IL-10 from (G) plasma at 7 DPI (H) and brain homogenate at 7 DPI, 1 MPI, and 12 MPI as measured by a multiplex immunoassay. Graphs represent pooled data from at least three individual animals. Mean ± the SEM. *, $p < 0.05$; **, $p < 0.01$; ***, $p < 0.001$. DPI = days post infection, MPI = months post infection. EU = ELISA units.

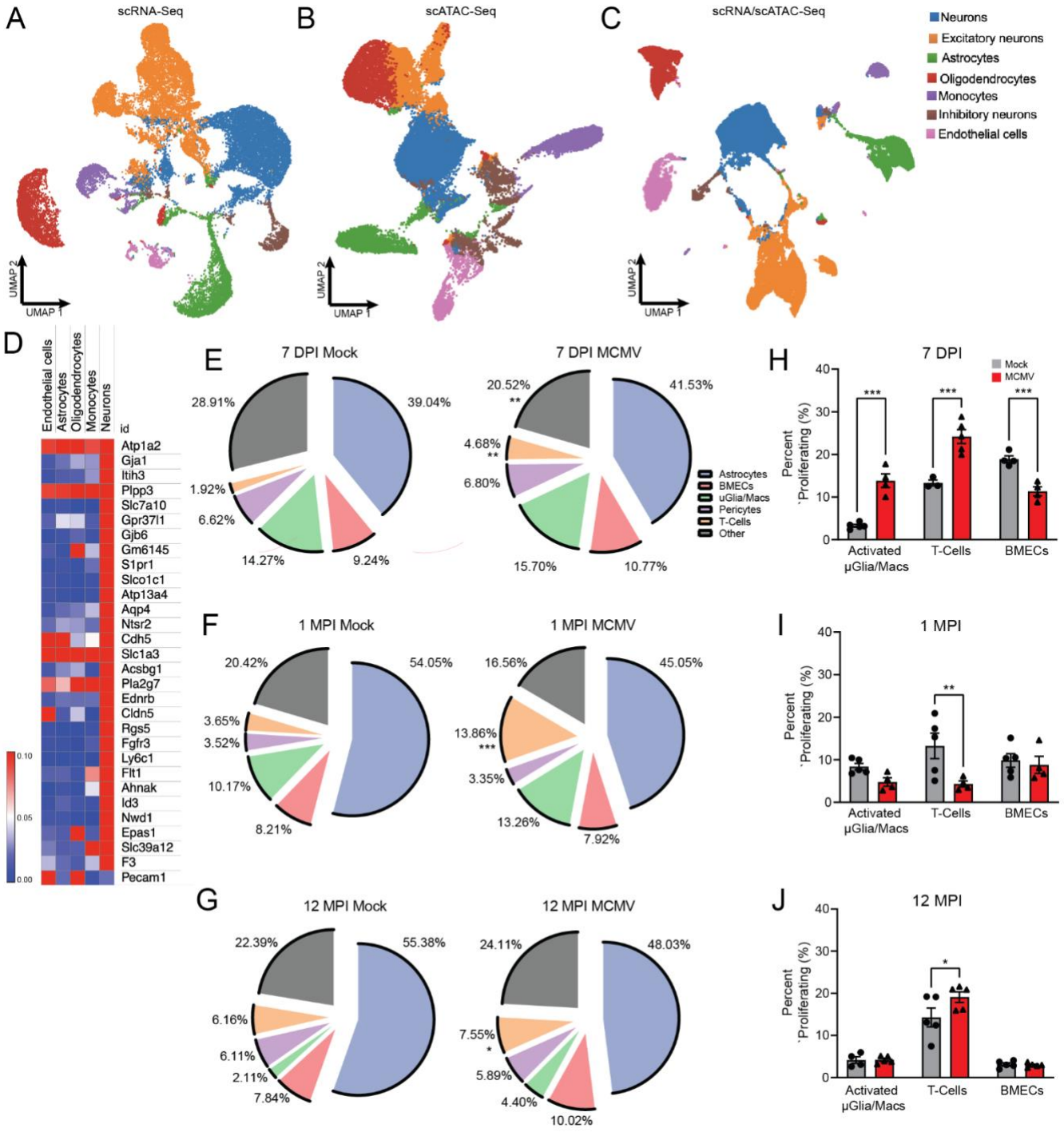

Figure 2: Intermittent MCMV infection alters the transcriptional profile of brain cells. Multiome libraries were generated and integrated. UMAP clustering of cell types based on single cell expression (A), chromatin accessibility (B) and integrated scATAC/scRNA (C). (D) Heatmap of transcriptional changes plotted by cell type. Population distributions as a percentage of live cells isolated in mock- and MCMV-infected mice at (E) 7 DPI, (F) 1 MPI, (G) 12 MPI as assessed by flow cytometry. Percentage of proliferating cells in different cell populations as measured by Ki-67 positivity at (H) 7DPI, (I) 1 MPI, and (J) 12 MPI. Graphs represent pooled data from at least three individual animals. Mean ± the SEM. *, $p < 0.05$; **, $p < 0.01$; ***, $p < 0.001$.

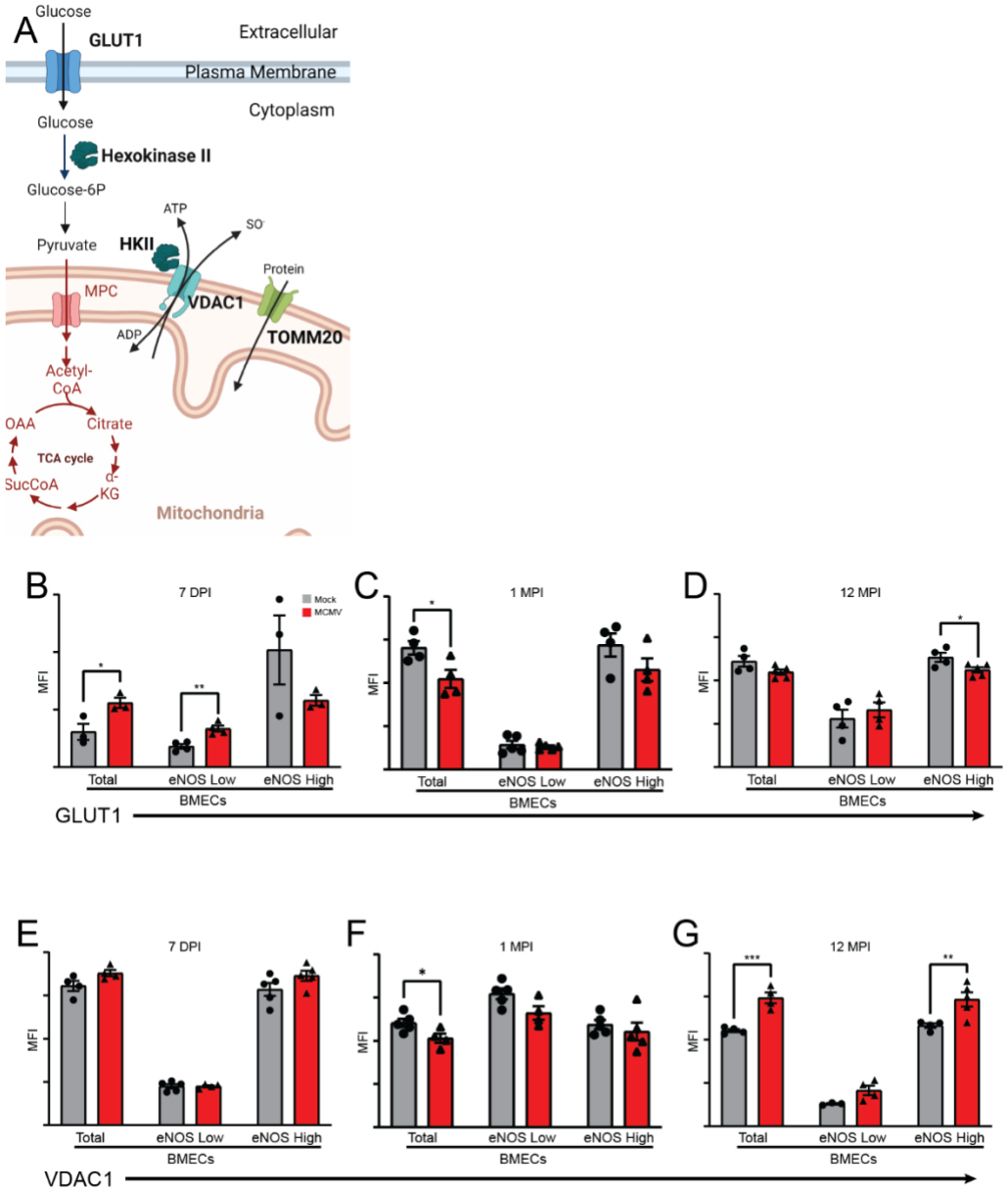

Figure 3: Blood brain barrier metabolic pathways are rewired with increased MCMV exposure. (A) Cartoon identifying key proteins in glycolysis and mitochondrial function. Flow cytometry was used to examine expression of GLUT1 in populations of BMECs at (B) 7 DPI, (C) 1 MPI, and (D) 12 MPI. Expression of VDAC1 in populations of BMECs at (E) 7 DPI, (F) 1 MPI, and (G) 12 MPI. Graphs represent pooled data from at least three individual animals. Mean ± the SEM. *, $p < 0.05$; **, $p < 0.01$; ***, $p < 0.001$. eNOS = endothelial nitric oxide synthase, MFI = mean fluorescent intensity.

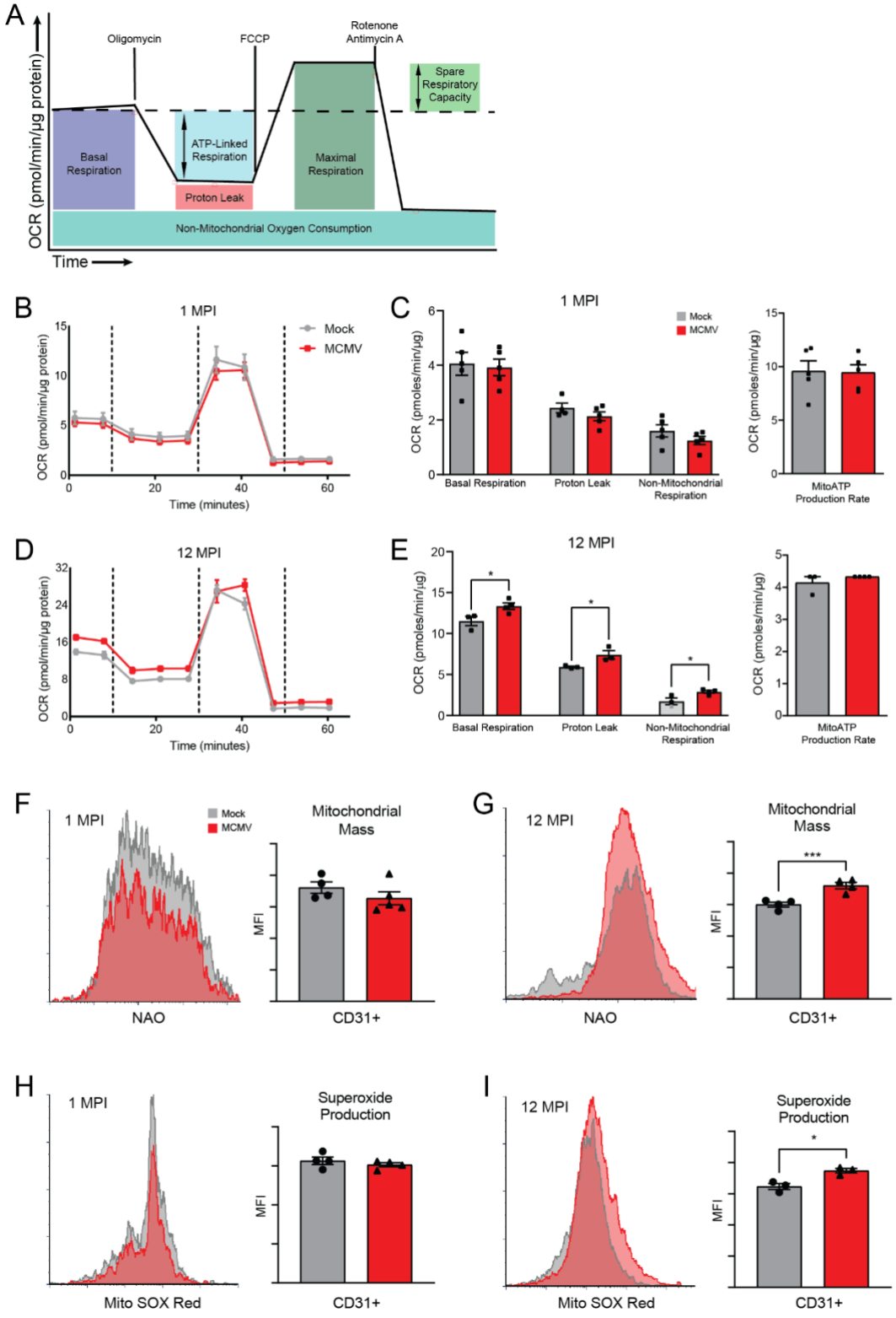

Figure 4: Hallmarks of mitochondrial dysfunction and oxidative stress are elevated in BMECs intermittently exposed to MCMV. (A) Cartoon illustrating how mitochondrial function was measured in BMECs using the Seahorse XFe24 MitoStress Kit. All samples were normalized to protein concentration. Representative data output of BMECs from the (B) 1 MPI and (D) 12 MPI timepoints. Basal Respiration, Proton Leak, Non-Mitochondrial Oxygen Consumption and mitochondrial ATP production rate were derived from the (C) 1 MPI and (E) 12 MPI measurements. Mitochondrial mass was determined by flow cytometry at (F) 1 MPI and (G) 12 MPI using nonyl acridine orange (NAO). Superoxide production was assessed using mitoSOX Red at (H) 1 MPI and (I) 12 MPI. Graphs represent pooled data from at least three individual animals. Mean ± the SEM. *, $p < 0.05$; **, $p < 0.01$; ***, $p < 0.001$. OCR = oxygen consumption rate, MPI = months post infection.

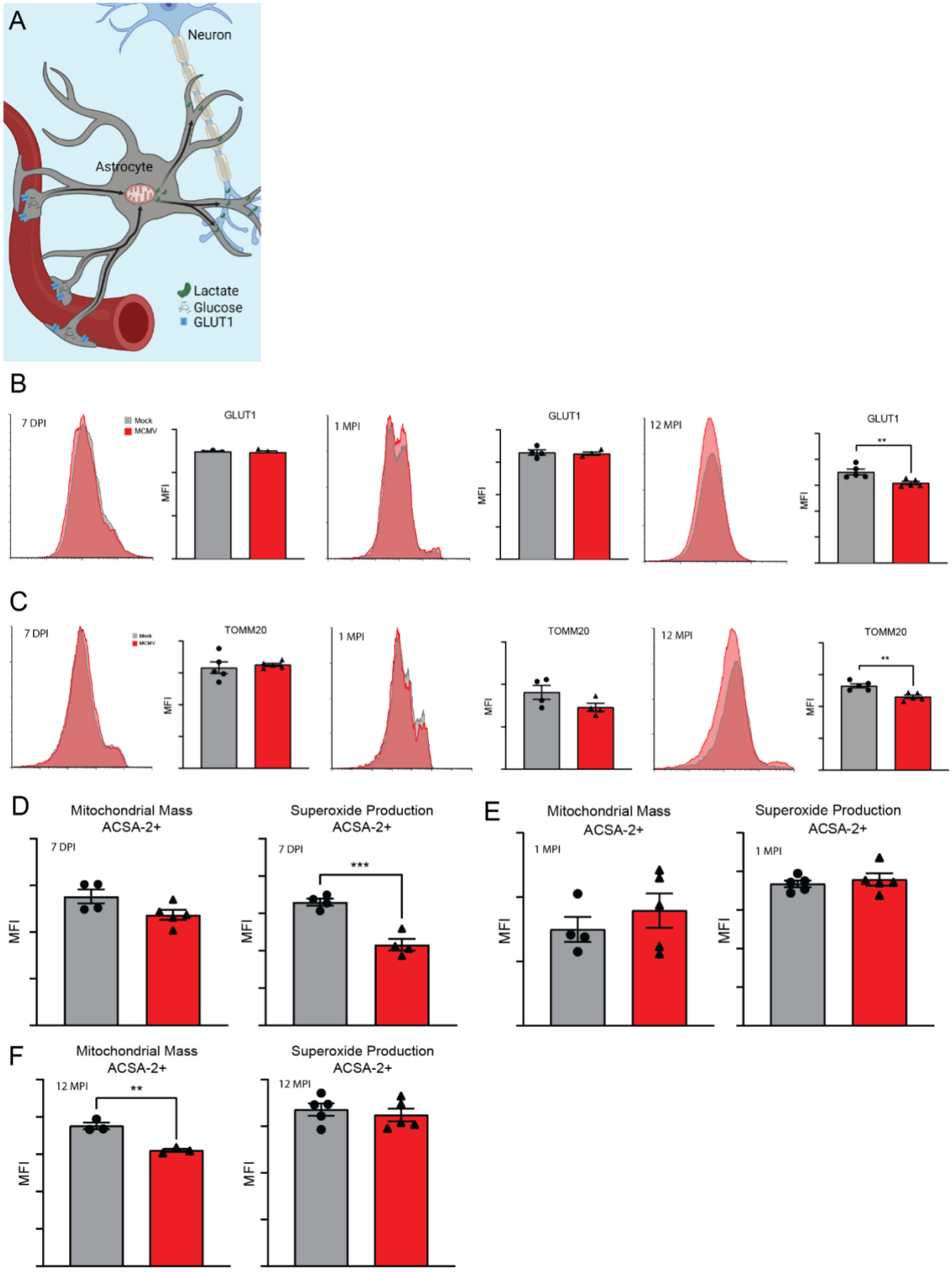

Figure 5: MCMV infection metabolically rewires astrocytes as a function of age. (A) Cartoon demonstrating the flow of metabolites from the bloodstream through astrocytes to neurons. Flow cytometry expression of (B) GLUT1 and (C) TOMM20 in astrocytes at 7 DPI, 1 MPI and 12 MPI. Mitochondrial mass and superoxide production were determined using nonyl acridine orange and mitoSOX red staining respectively and are quantified at (5D) 7 DPI, (5E) 1 MPI, and (5F) 12 MPI. Graphs represent pooled data from at least three individual animals. Mean ± the SEM. *, $p < 0.05$; **, $p < 0.01$; ***, $p < 0.001$. DPI = days post infection, MPI = months post infection. ACSA-2 = astrocyte cell surface antigen 2.

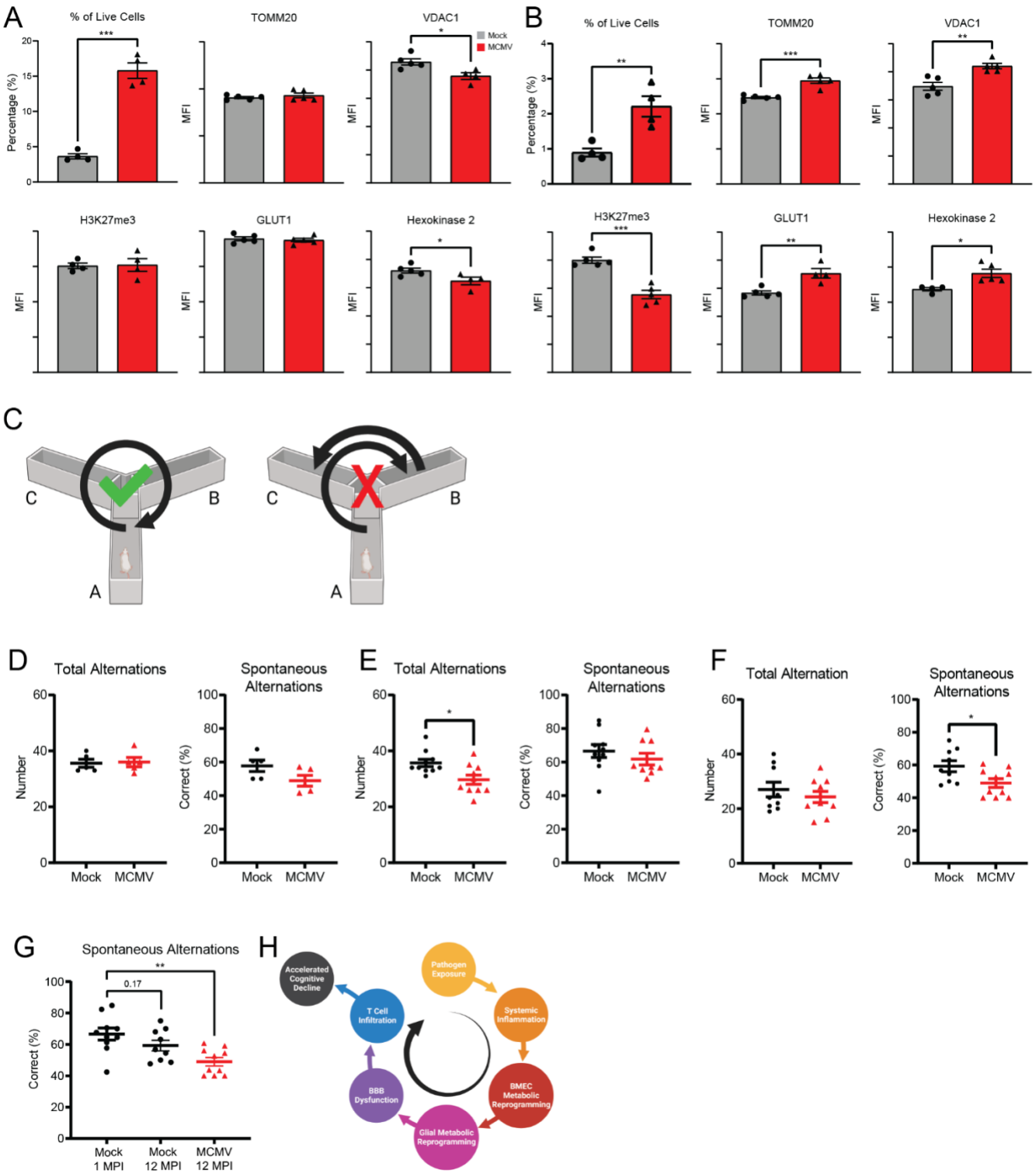

Figure 6: Cognition is impaired with intermittent MCMV infection. Proliferation, epigenetic, and metabolic markers of CNS resident T cells were examined using flow cytometry at (A) 1 MPI and (B) 12 MPI. (C) Schematic describing correct versus incorrect alternations in the Y-maze. Quantification of number of alternations and percentage of spontaneous correct alternations at (D) 7 DPI, (E) 1 MPI, and (F) 12 MPI mice. (G) Comparison of spontaneous alternations examining the interactions between age and infection status. (H) Diagram presenting the model of pathogen associated accelerated cognitive aging. Graphs represent pooled data from at least three individual animals. Mean ± the SEM. *, $p < 0.05$; **, $p < 0.01$; ***, $p < 0.001$. MPI = months post infection, MFI = mean fluorescent intensity.

Marker	Color/Format
Ki67	BV421
TOMM20	AF405
GBP2	CF405M
CD3	BV510
Live/Dead	Yellow 575
CD31	BV605
CD11b	BV650
CD206	BV711
CD45.2	BV750
eNOS3	AF488
GFAP	Alexa Fluor 532
H3K27me3	PE
Claudin-5	PE-Texas Red
iNOS2	PE-Atto 594
Hexokinase 2	PerCP-Cy5.5
CD86	PE-Vio770
ACSA2	APC
GLUT-1	Alexa Fluor 647
CD163	AF680
S100A10(p11)	AF700
VDAC1	APC-Cy7
NG2	AF790

Table S1: Antibodies and fluorophores.

Supplemental Figure 1: Intermittent MCMV infection exhibits delayed inflammatory cytokine expression in the brain. (A) Weight change in mock- and MCMV-infected mice over 7 DPI from initial infection through the 9-month infection time point. (B) Monthly weight of animals from initial infection through 12 MPI. (C) Agarose gel displaying UL123 qRT-PCR products from salivary glands at 7 DPI, 1 MPI, 6 MPI, and 12 MPI. Cytokine levels from (D) plasma at 7 DPI and (E) brain homogenate at 7 DPI, 1 MPI, and 12 MPI as measured by a multiplex immunoassay. Cytokine levels in (F) plasma at 1 and 12 MPI, and (G) brain homogenate in mock infected animals at 7 DPI, 1 MPI, and 12 MPI. Graphs represent pooled data from at least three individual animals. Mean ± the SEM. *, $p < 0.05$; **, $p < 0.01$; ***, $p < 0.001$. DPI = days post infection, MPI = months post infection.

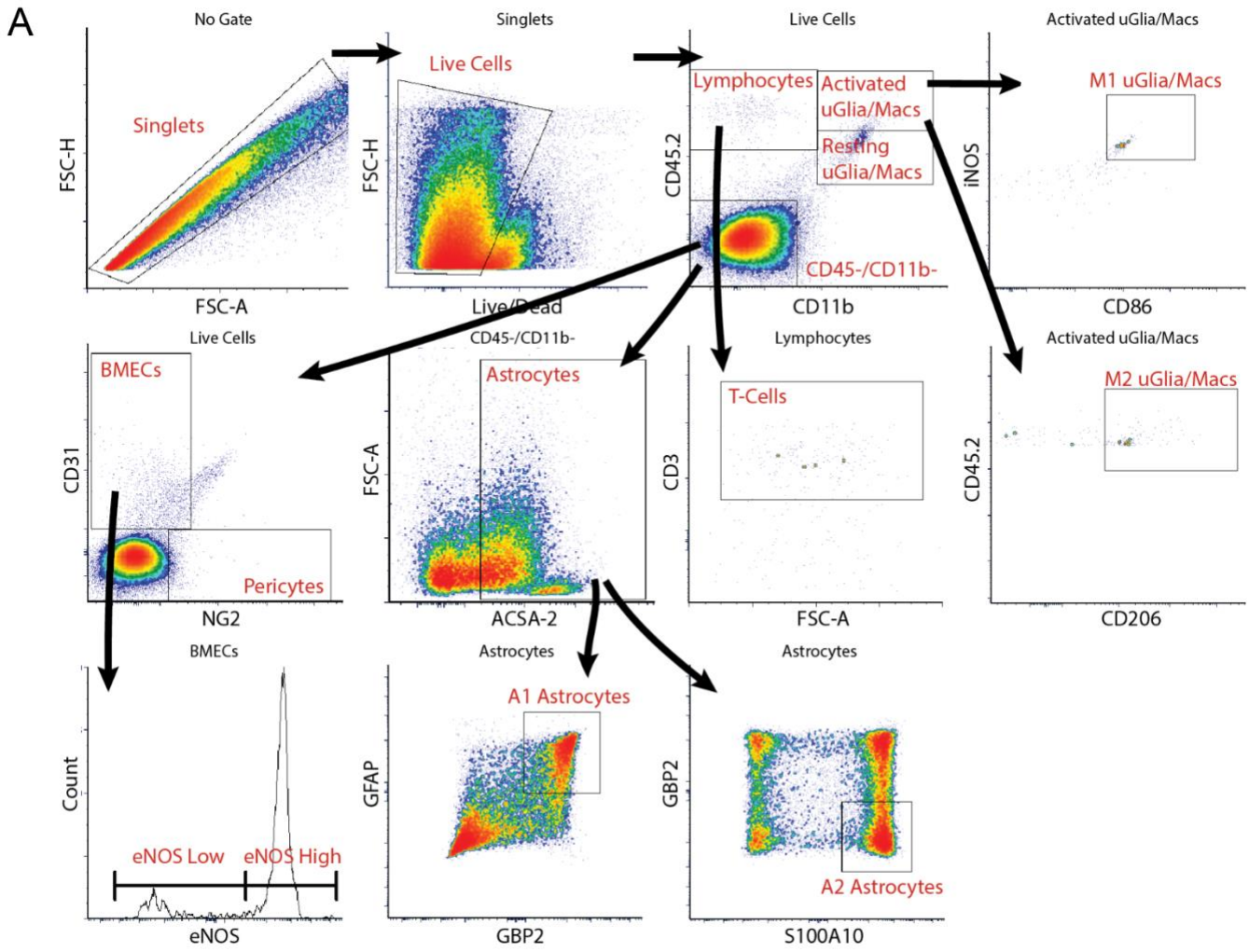

Figure S2: Brain phenotyping flow cytometry panel gating strategy.

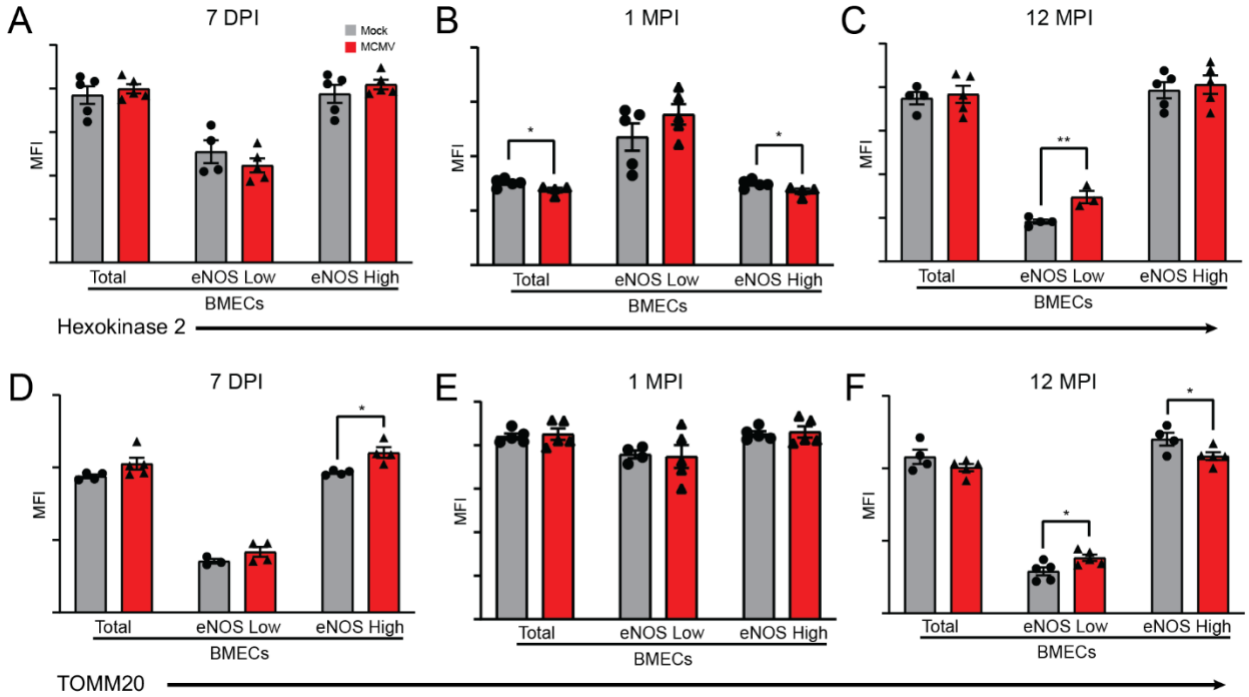

Figure S3: Blood brain barrier metabolic pathways are rewired with increased MCMV exposure. Flow cytometry was used to examine expression of Hexokinase 2 in populations of BMECs at (A) 7 DPI, (B) 1 MPI, and (C) 12 MPI. Expression of TOMM20 in populations of BMECs at (D) 7 DPI, (E) 1 MPI, and (F) 12 MPI. Graphs represent pooled data from at least three individual animals. Mean ± the SEM. *, $p < 0.05$; **, $p < 0.01$; ***, $p < 0.001$. eNOS = endothelial nitric oxide synthase, MFI = mean fluorescent intensity.

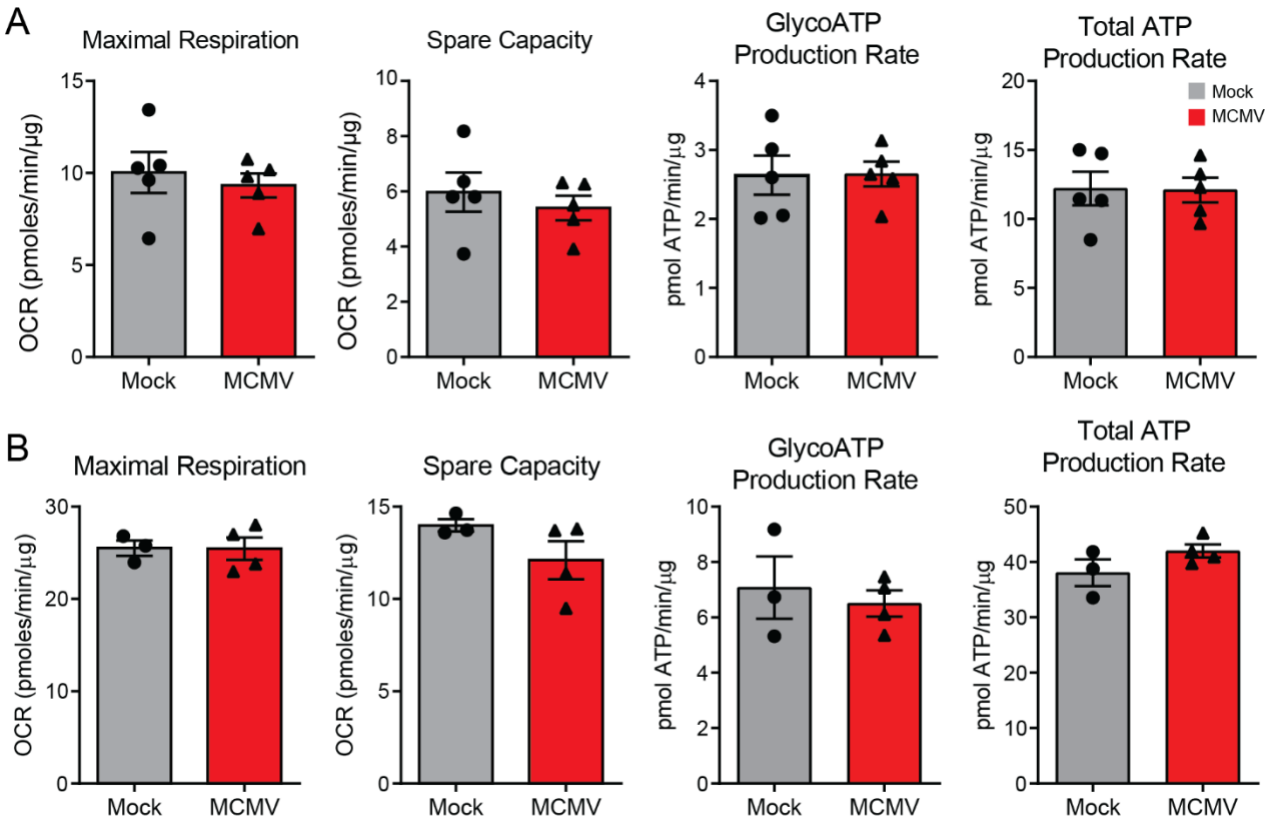

Figure S4: Hallmarks of mitochondrial dysfunction and oxidative stress are elevated in BMECs intermittently exposed to MCMV. Maximal Respiration, Spare Respiratory Capacity, GlycoATP Production Rate, and Total ATP Production Rate were derived from the (S4A) 1 MPI and (S4B) 12 MPI measurements. Graphs represent pooled data from at least three individual animals. Mean ± the SEM. OCR = oxygen consumption rate.

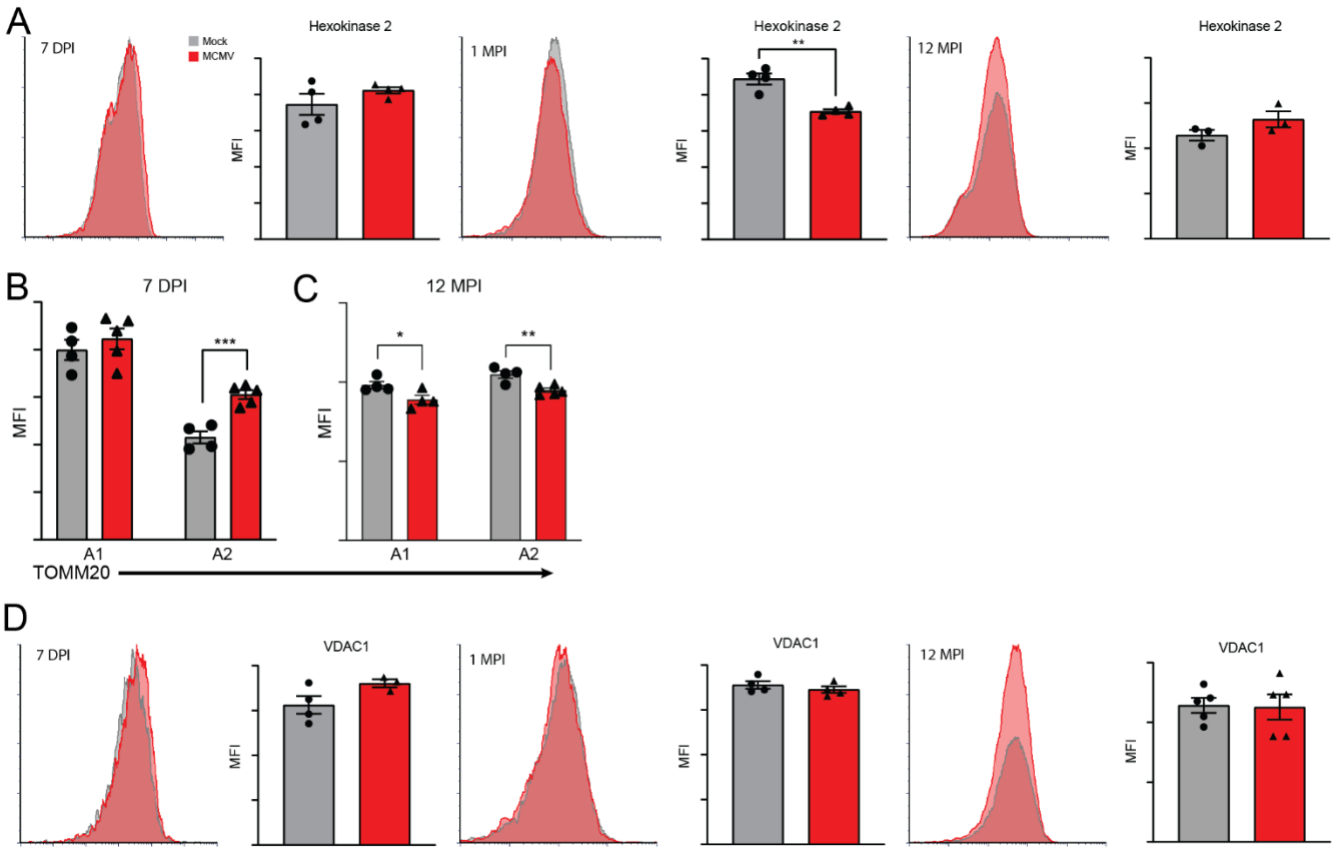

Figure S5: MCMV infection metabolically rewires astrocytes as a function of age. Flow cytometry expression of (A) Hexokinase 2 in astrocytes at 7 DPI, 1 MPI and 12 MPI. TOMM20 expression in A1 and A2 astrocytes at (B) 7 DPI and (C) 12 MPI. (D) VDAC1 expression in astrocytes at 7 DPI, 1 MPI, and 12 MPI. Graphs represent pooled data from at least three individual animals. Mean ± the SEM. *, $p < 0.05$; **, $p < 0.01$; ***, $p < 0.001$. DPI = days post infection, MPI = months post infection, MFI = mean fluorescent intensity.

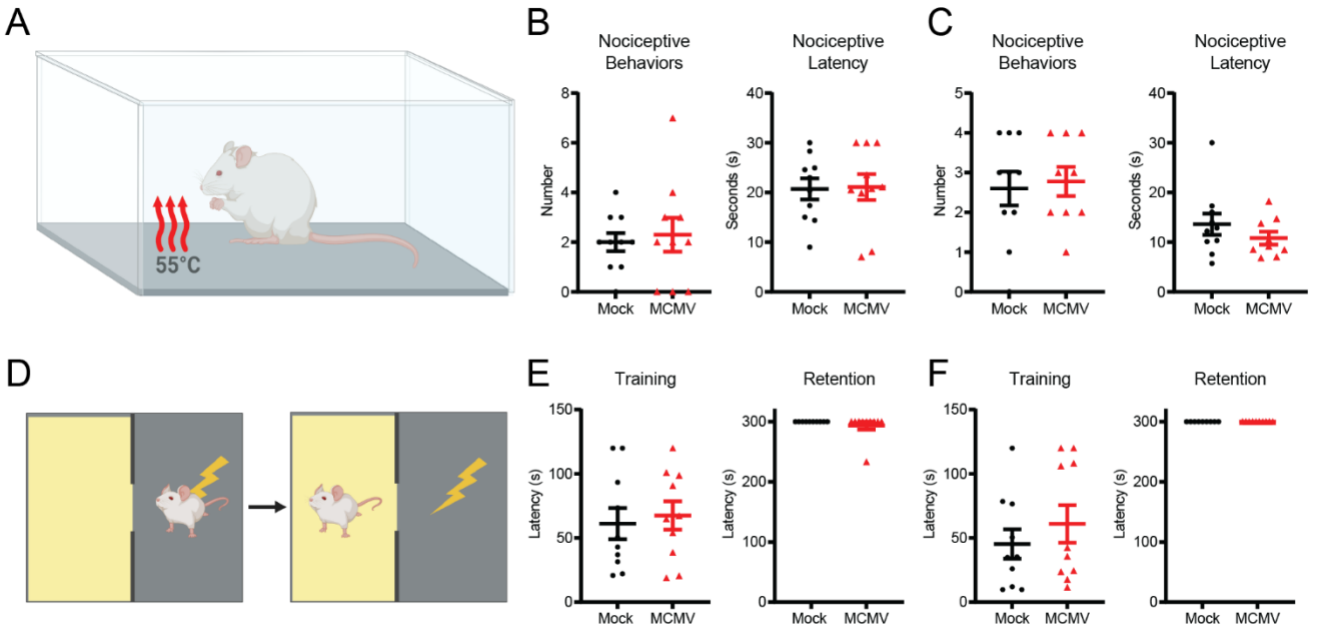

Figure S6: Cognition is impaired with intermittent MCMV infection. (A) Cartoon of the hot plate assay. Quantification of the number and latency to produce nociceptive behaviors in the hot plate assay at (B) 1 MPI and (C) 12 MPI. (D) Cartoon of the passive avoidance foot shock assay. Quantification of latency to enter the dark, foot-shock chamber during training and 24-hour retention testing in (E) 1 MPI (F) 12 MPI animals. Graphs represent pooled data from at least three individual animals. Mean ± the SEM. *, $p < 0.05$; **, $p < 0.01$; ***, $p < 0.001$.

VIRUS PROPAGATION AND QUANTIFICATION

Murine cytomegalovirus (MCMV) Smith strain was passaged through mice and quantified via plaque assay as previously described (Brune et al., 2001; Zurbach et al., 2014). Briefly, mice were i.p. injected with MCMV and sacrificed at 14 days post infection. Salivary glands were homogenized in PBS, aliquoted, and stored at -80°C. Virus was quantified by plaque assay using M2-10B4 cells and a viscous overlay followed by fixation with formaldehyde and staining with 0.02% methylene blue.

ANIMALS, INFECTIONS, AND SAMPLE COLLECTIONS

Female BALB/cJ mice aged 6 weeks were obtained from Charles River and housed in disposable, sterile cages in groups of 5 with food and water provided *ad libitum*. All animal experiments were approved by the Tulane University Institutional Animal Care and Use Committee. MCMV infections were conducted via i.p. injection with $5x10^4$ plaque forming units in 100uL sterile PBS. They were maintained on a diurnal light cycle (8-6). Mice were euthanized via i.p. injection with a sub-lethal dose of ketamine and xylazine followed by exsanguination. Blood collected via cardiac puncture was processed for plasma. Mice were then perfused with ice-cold PBS and tissues were collected and processed as needed.

BEHAVIORAL TESTING

Behavior in mice was evaluated using the Y-maze, Passive Avoidance, and Hot Plate tasks at 1 month post initial infection or 12 months post initial infection. The behavior tests described below were performed in the order they are listed. All behavioral testing was performed between 0800 and 1400 hrs. All animals underwent testing by a pair of treatment blinded researchers. Peroxiguard was used to disinfect and deodorize the apparatuses between each mouse trial.

Y-Maze: The Y-Maze was employed as a measurement of spontaneous alternation/short-term recognition memory (Swonger and Rech, 1972). Mice were placed in the three-armed maze with arm length of 38 cm, width of 8.25 cm, and height of 13.25 cm facing the end of arm designated “A”. Mice were allowed to freely explore the maze for 8 minutes. Movement around the maze was recorded by an overhead camera and tracked using ANY-Maze 7.1 software. Mice were provided with large black geometric spatial clues on white backgrounds to help them navigate and discriminate between arms. Spontaneous alternation was calculated as percentage of correct alternations between the three arms without revisiting the previous arm. Total alternation (number of total arm entries minus 2).

Passive Avoidance: As a measure of single-trial fear based aversive learning, mice were subjected to the step-through inhibitory (passive) avoidance task (Jarvik and Kopp, 1967). In this assay mice are placed in a two-chamber device with a guillotine door between them. One chamber is brightly lit while the other is dark. The floor of both chambers contains metal rungs on the floor connected to a shock delivery apparatus (Maze Engineers). For the training portion of the test, mice were placed in the brightly illuminated side (approx.. 1300 lux) and allowed to explore until they entered the dark chamber. Once the mouse entered the dark chamber the door was closed and the mouse was administered a 2 second foot shock (0.25 mA). Mice that did not enter the dark chamber within 120 seconds were gently pushed to the dark chamber and a foot shock was administered. After the training trial was completed, animals were tested for learning ability (10 minutes after training trial) and memory retention (24 hours later) by placing the mice

in the bright chamber and recording latency to enter dark chamber. These retention trials were limited to 300 seconds.

Hot Plate: To examine nociceptive ability, mice were exposed to the hot plate test (Woolfe and Macdonald, 1944). The hot plate (Maze Engineers) was set to 55.0°C and the mouse was placed onto the plate surface. Latency to first nociceptive behavior as well as total number of nociceptive behaviors was recorded for the 30 second duration of the experiment. Nociceptive behaviors were defined as shaking or flicking of hindlimbs and jumping.

SINGLE CELL MULTIOME ATAC AND GENE EXPRESSION SEQUENCING

Nuclei Isolation: Nuclei isolation for multiome sequencing was performed following protocol revision D (10X Genomics) with minor modifications. Following euthanasia and perfusion, the brain was extracted and flash frozen in liquid nitrogen. The brain was lysed with 0.1x lysis buffer and homogenized with scissors and a pellet pestle. Homogenate was then incubated for 3 minutes on ice and lysis stopped via the addition of wash buffer. The suspension was filtered through a 70 µm filter and then subjected to a 30% Percoll Plus centrifugation to remove myelin. Nuclei were washed and resuspended in nuclei buffer. Finally, nuclei were visualized on a cell counter for nuclear membrane integrity (lack of blebbing) and counting.

Library Prep and Sequencing: The Chromium Next GEM Single Cell Multiome ATAC and GEX protocol (CG000338) and 10x reagent kit were used to prepare ~10,000 nuclei/sample for the Multiome sequencing. Briefly, nuclei suspensions were incubated with a Transposon Mix and DNA fragments were transposed and barcoded. The transposed nuclei were partitioned into nanoliter-scale Gel Bead-In EMulsion (GEMs). The barcoded transposed DNA and barcoded full-length cDNA from poly-adenylated mRNA were generated and amplified by PCR. P7 and a sample index were added to transposed DNA during ATAC library construction via PCR. Barcoded cDNA enzymatic fragmentation, end-repair, A-tailing, and adaptor ligation were followed by PCR amplification. Both final ATAC libraries and 3′ Gene Expression libraries generated contained standard Illumina P5 and P7 paired-end constructs. Library quality controls were performed by using an Agilent High Sensitivity DNA kit with Agilent 2100 Bioanalyzer and quantified by Qubit 2.0 fluorometer. Libraries were sequenced separately with individual parameter settings. Pooled libraries at 650 pM were sequenced with paired end dual index configuration on an Illumina NextSeq 2000 using Illumina P3 100 cycle kit. Cell Ranger arc version 2.0.0 (10X Genomics) was used to process raw sequencing data and mapped to mouse genome mm10-2020-A to generate differentially expressed genes between specified cell clusters represented by Loupe Cell Browser (10X Genomics).

Multiome Data Analysis: Cell Ranger ARC v2.0 (10x Genomics) was used to process raw sequencing data for further downstream analyses. After filtering, we used 27,798 cells with high quality transcriptome and epigenome profiles. We followed the algorithms Seurat (v4.0) R package (v4.0.2) to generate the uniform manifold approximation and projection (UMAP) embeddings and differentially expressed (DE) gene. Fragment files were used as input for Seurat analysis. The input fragment file was processed as chunks per chromosome and stored in HDF5 format (hierarchical data format version 5), allowing rapid access and efficient read and write functions during analysis. The quality control steps involved the removal of all low-quality cells and predicted heterotypic doublets from our analysis. We used Morpheus (https://software.broadinstitute.org/morpheus/) software to generate the top 30 DE genes

heatmap. A relative color scheme uses the minimum 0 and maximum 0.1 values in each row to convert values to colors.

RNA ISOLATION AND qRT-PCR

Salivary glands were flash frozen in liquid nitrogen and stored at -80°C. RNA was isolated from 30 mg of salivary gland using the RNeasy minikit from Qiagen. iScript cDNA synthesis kit was used to created cDNA from 1 ug of RNA. qRT-PCR was conducted on 50 ng of each sample using Sso Advanced SYBR Green Supermix and primers for MCMV immediate early gene 1 (UL123) and murine 36B4 which was used as a housekeeping gene. qPCR products were run on a 2% agarose gel to confirm product size.

FLOW CYTOMETRY

Brains were processed for flow cytometry as previously described (Calvo et al., 2020). Briefly, they were incubated with 5mg collagenase II and homogenized in MACS C-tubes with 5 mg collagenase II and 100U DNAse I in HBSS with 3mM calcium chloride. Myelin debris was removed via a 30% Percoll Plus gradient. Cells were washed and resuspended in PBS with 0.4% BSA.

Neuro Flow Panel: Cells were incubated with fixable live dead stain and Fc block for 15 minutes at RT. Following washes with 20% BD Horizon Brilliant Stain Buffer, cells were incubated in an extracellular antibody cocktail for 20 minutes at RT. Cells were washed, fixed and permeabilized with eBioscience FoxP3 Transcription Factor staining kit for 45 minutes. Fixed cells were washed and incubated with intracellular antibodies for 45 minutes at room temperature. Following washes, cells were resuspended in PBS with 0.5% BSA and flow cytometry was conducted on a Cytek Aurora. Data was analyzed using FCS Express 7.14.

Live Cell Mitochondrial Panel: Cells were incubated in a cocktail of anti-CD31 BV605 antibody at 1:100, 1 μM nonyl acridine orange (mitochondrial mass), 2.5 μM MitoSOX Red (superoxide production), and 250 nM MitoTracker Red FM (mitochondrial membrane potential) for 45 minutes at 37°C. Following washes in PBS, cells were resuspended in PBS with Sytox Blue dead cell stain, incubated for 15 minutes, and flow cytometry was performed on a BD LSRFortessa. Data was analyzed using FCS Express 7.14.

CYTOKINE ANALYSIS

Mouse brains were minced briefly in BioRad Cell Lysis Buffer followed by homogenization in MACS S-tubes and freezing at -80°C. Following thaw, lysate was sonicated briefly and then centrifuged to pellet debris before being quantified by BCA. Brain lysate was diluted to 4mg/mL in Bio-Plex diluent.

Both plasma and brain lysate cytokine levels were assessed using a Bio-Plex murine cytokine 23-plex assay kit at a dilution of 1:2 according to manufacturer recommendations. Briefly, samples were added to a 96-well plate with magnetic beads and incubated for 30 minutes while shaking. Well, were washed three times and followed by addition of detection antibodies for 30 minutes at room temperature. Three more washes were conducted and then streptavidin-PE was added and incubated for 10 minutes. After another three washes samples were read on the Bio-Plex 200 system with HTF. Standard curves were created for each cytokine from 1-32,000 pg/mL, a five-parameter logistic regression was fit, and sample cytokine concentrations were interpolated.

ELISA

Antigen-specific quantitative ELISAs were performed using similar methods as described in ref. (Norton et al., 2015). Briefly, 96-well plates were coated with 0.25 µg/well of UV-inactivated MCMV. Serial dilutions of plasma from animals were incubated for an hour at room temperature followed by detection using AP-conjugated rabbit anti-mouse IgG or IgM. ELISAs were quantified using dilutions of purified mouse standards IgG1-κ or IgM-κ and the results were expressed as ELISA units/mL (EU/mL).

BRAIN MICROVESSEL ISOLATION

Excised brains were stored in ice-cold PBS. Brain microvessels (BMVs) were isolated as previously described {Sakamuri, 2022 #1160;Sakamuri, 2022 #1218}. Briefly, hemispheres were rolled on filter paper to remove surface vessels. Brains were homogenized in PBS, centrifuged, and the pellet was resuspended in 17.5% dextran solution. This process was repeated, and each time floating white matter was removed from the pellet prior to resuspension. The resuspended vessels were serially filtered through a 300 µm and 40 µm filters and then the BMV pellet is resuspended in Seahorse XF DMEM media.

SEAHORSE

BMVs were loaded into Seahorse XFe24 cell plates with one mouse used for each well. Plates were centrifuged and incubated for 1 hour at 37°C in a non-CO_2 incubator. Mitochondrial function was assessed using the Mito Stress Test Kit. Basal media contained 25 mM glucose, 10 mM sodium pyruvate, and 2 mM glutamate. The assay was completed using the manufacturers recommended protocols with following injections: Oligomycin (5 µM), FCCP (5 µM), and Rotenone/Antimycin A (2 µM/10 µM). Total protein per well was determined via BCA and oxygen consumption rates were normalized to total protein for each well. Normalized OCR was used to determine basal and maximal respiration, ATP coupled respiration, proton leak, and spare respiratory capacity.

STATISTICAL ANALYSIS

Statistical analyses were performed using Graphpad Prism v9. All data are expressed as the mean plus standard error of the mean (SEM) from at least three independent experiments or animals. Comparisons between groups were assessed using unpaired *t*-tests, ordinary one-way ANOVA, or repeated measures ANOVA followed by Dunett's multiple comparisons test where appropriate. Outliers were identified and excluded where necessary using the ROUT method with a maximum desired false discovery rate (Q) of 2%. For all comparisons, a $p < 0.05$ was considered significant.

Brune, W., Hengel, H., and Koszinowski, U.H. (2001). A mouse model for cytomegalovirus infection. Curr Protoc Immunol *Chapter 19,* Unit 19 17.

Calvo, B., Rubio, F., Fernandez, M., and Tranque, P. (2020). Dissociation of neonatal and adult mice brain for simultaneous analysis of microglia, astrocytes and infiltrating lymphocytes by flow cytometry. IBRO Rep *8*, 36-47.

Jarvik, M.E., and Kopp, R. (1967). An improved one-trial passive avoidance learning situation. Psychol Rep *21*, 221-224.

Norton, E.B., Bauer, D.L., Weldon, W.C., Oberste, M.S., Lawson, L.B., and Clements, J.D. (2015). The novel adjuvant dmLT promotes dose sparing, mucosal immunity and longevity of antibody responses to the inactivated polio vaccine in a murine model. Vaccine *33*, 1909-1915.

Sakamuri, S.S., Sure, V.N., Kolli, L., Evans, W.R., Sperling, J.A., Bix, G.J., Wang, X., Atochin, D.N., Murfee, W.L., Mostany, R., et al. (2022). Aging related impairment of brain microvascular bioenergetics involves oxidative phosphorylation and glycolytic pathways. J Cereb Blood Flow Metab *42*, 1410-1424.

Swonger, A.K., and Rech, R.H. (1972). Serotonergic and cholinergic involvement in habituation of activity and spontaneous alternation of rats in a Y maze. J Comp Physiol Psychol *81*, 509-522.

Woolfe, G., and Macdonald, A.D. (1944). THE EVALUATION OF THE ANALGESIC ACTION OF PETHIDINE HYDROCHLORIDE (DEMEROL). Journal of Pharmacology and Experimental Therapeutics *80*, 300.

Zurbach, K.A., Moghbeli, T., and Snyder, C.M. (2014). Resolving the titer of murine cytomegalovirus by plaque assay using the M2-10B4 cell line and a low viscosity overlay. Virol J *11*, 71.

KEY RESOURCES TABLE

REAGENT or RESOURCE	SOURCE	IDENTIFIER
Antibodies		
Rat monoclonal anti-Ki-67 (clone 11F6)	BioLegend	Cat# 151208; RRID:AB_2629748
Rabbit recombinant anti-TOMM20 (clone EPR15581-54)	abcam	Cat# ab186735; RRID:AB_2889972
Rabbit polyclonal anti-GBP2	Biorbyt	Cat# orb763167
Rat monoclonal anti-CD3 (clone 17a2)	BioLegend	Cat# 100234; RRID:AB_2562555
Rat monoclonal anti-CD31 (clone 390)	BioLegend	Cat# 102427; RRID:AB_2563982
Rat monoclonal anti-CD11b (clone M1/70)	BioLegend	Cat# 101259; RRID:AB_2566568
Rat monoclonal anti-CD206 (clone C068C2)	BioLegend	Cat# 141727; RRID:AB_2565822
Mouse monoclonal anti-CD45.2 (clone 104)	BioLegend	Cat# 109857; RRID:AB_2832376
Mouse monoclonal anti-NOS3	Santa Cruz Biotechnology	Cat# sc-376751; RRID:AB_2832203
Mouse monoclonal anti-GFAP (clone spm248)	Novus Biologicals	Cat# NBP2-34401AF532
Rabbit monoclonal anti-Tri-Methyl-Histone H3 (Lys27) (clone C36B11)	Cell Signaling Technology	Cat# 40724; RRID:AB_2799182
Mouse monoclonal anti-Claudin 5 (clone 4C3C2)	Thermo Fisher Scientific	Cat# 35-2500; RRID:AB_2533200
Rat monoclonal anti-Nos2 (clone W16030C)	BioLegend	Cat# 696802; RRID:AB_2687097
Rabbit recombinant anti-Hexokinase II (clone EPR20839)	Abcam	Cat# ab228819; RRID:AB_2868547
Rat monoclonal anti-CD86 (clone PO3.3)	Miltenyi Biotec	Cat# 130-105-135; RRID:AB_2660750
Rat monoclonal anti-ACSA-2 (clone IH3-18A3)	Miltenyi Biotec	Cat# 130-117-535; RRID:AB_2727978
Rabbit monoclonal anti-Glucose Transporter GLUT1 (clone EPR3915)	Abcam	Cat# ab195020; RRID:AB_2783877
Rabbit polyclonal anti-CD163/M130	Bioss	Cat# bs-2527R; RRID:AB_10856166
Mouse recombinant anti-S100A10	biotechne	Cat# FAB2377N
Mouse monoclonal anti-VDAC1/Porin (clone 20B12)	Abcam	Cat# ab14734; RRID:AB_443084
Mouse monoclonal anti-NG2 (clone G-9)	Santa Cruz Biotechnology	Cat# sc-166251; RRID:AB_2261269
Rabbit Anti-mouse IgG AP	Sigma	A1902
Goat Anti-mouse IgM AP	Southern Biotech	Cat# 1021-04
Bacterial and virus strains		
Murine Cytomegalovirus Smith Strain	ATCC	VR-1399
Chemicals, peptides, and recombinant proteins		
Collagenase II	Cell Signaling Technologies	CST #77336
Sodium Carbonate	Sigma	S2127
Sodium Bicarbonate	Sigma	S8875

Sodium Azide	Sigma	S2002
Magnesuim chloride hexahydrate	Sigma	M2773
Diethanolamine	Sigma	D8885
IgG1, Kappa from murine myeloma	Sigma	M9269
IgM, Kappa from murine myeloma	Sigma	M3795
4-Nitrophenyl phosphate disodium salt hexahydrate	Sigma	N2765
Percoll PLUS	Cytiva	#17544502
DNase 1	Worthington Biochem	LS006333
Ketaset	Zoetis	
AnaSed LA	Vet One	13985-704-10
Bovine Serum Albumin	Sigma Aldrich	A9418-100G
iScript cDNA Synthesis Kit	Bio-Rad	Cat #1708891
SsoAdvanced Universal SYBR Green Supermix	Bio-Rad	Cat #1725271
Live/Dead Fixable Yellow dead cell stain	Thermo Fisher Scientific	L34959
Brilliant Stain Buffer Plus	BD Biosciences	Cat# 566385
eBioscience Fixation/Permeabilization Concentrate	Invitrogen	Cat# 00-5123-43
eBioscience Fixation/Permeabilization Diluent	Invitrogen	Cat# 00-5223-56
eBioscience Permeabilization Buffer (10X)	Invitrogen	Cat# 00-8333-56
Peroxiguard Disinfectant	Lighthouse Life Sciences	
UltraComp eBeads Plus Compensation Beads	Invitrogen	Cat# 01-3333-42
Seahorse XF DMEM medium, pH 7.4, 500 mL.	Agilent	103575-100
DMEM, high glucose	Thermo	11965092
Fetal Bovine Serum Premium Select	R&D Systems	S11550
Tween-20	Fisher Scientific	BP337-500
Certified Molecular Biology Agarose	Bio-Rad	Cat #161-3100
5x DNA Loading Buffer Blue	Meridian Bioscience	Cat #BIO-37045
SYBR™ Safe DNA Gel Stain	Thermo Fisher Scientific	Cat# S33102
ACK Lysing Buffer	Thermo Fisher Scientific	Cat# A1049201
UltraPure™ 0.5M EDTA, pH 8.0	Thermo Fisher Scientific	Cat# 15575020
SYTOX™ Blue Nucleic Acid Stain - 5 mM Solution in DMSO	Thermo Fisher Scientific	S11348
MitoTracker™ Red FM Dye, for flow cytometry	Thermo Fisher Scientific	M46751
MitoSOX™ Mitochondrial Superoxide Indicators, for live-cell imaging	Thermo Fisher Scientific	M36008
Nonyl Acridine Orange (Acridine Orange 10-Nonyl Bromide)	Thermo Fisher Scientific	A1372
GlutaMAX Supplement	Thermo Fisher Scientific	35050061
16% Formaldehyde Solution Methanol-Free	Thermo Fisher Scientific	Cat# 28906
Methylene Blue (Certified Biological Stain), Fisher Chemical™	Fisher Scientific	M291-25
Critical commercial assays		
Micro BCA Protein Assay Kit	Thermo Fisher Scientific	Cat# 23235

Bio-Plex Pro Mouse Cytokine Grp I Panel 23-Plex	Bio-Rad	Cat #M60009RDPD
Bio-Plex Cell Lysis Kit	Bio-Rad	Cat #A1049201
Chromium Next GEM Single Cell Multiome ATAC + Gene Expression Reagent Bundle	10X Genomics	Cat #1000283
NextSeq 2000 P3 Reagents (100 Cycles)	Illumina	Cat #20040559
High Sensitivity DNA Kit	Agilent	Cat #5067-4626
Seahorse Mito Stress Test	Agilent	Cat #103015-100
RNeasy Mini Kit (250)	Qiagen	Cat# 74106
Deposited data		
Multiome Data	GeoAccesion	Number Pending
Experimental models: Cell lines		
M2-10B4	ATCC	CRL-1972
Experimental models: Organisms/strains		
Mouse: BALB/cAnNCrl	Charles River	Cat #028
Oligonucleotides		
Primer: m36B4 Forward 5'-CGACCTGGAAGTCCAACTAC-3'	Griessl et al. (2017)	
Primer: m36B4 Reverse 5'-ATCTGCTGCATCTGCTTG-3'	Griessl et al. (2017)	
Primer: mUL123 Forward 5'-TCAGCCATCAACTCTGCTACCAAC-3'	Tang-Feldman et al. (2006)	
Primer: mUL123 Reverse 5'-ATCTGAAACAGCCGTATATCATCTTG-3'	Tang-Feldman et al. (2006)	
Software and algorithms		
Gen5 v3.11	Agilent	
Wave v2.6.1.53	Agilent	
ANY-maze v7.1	ANY-maze	
CFX Maestro v4.1.2433.1219	Bio-Rad	
Bioplex Manager v6.1	Bio-Rad	
SpectroFlo v3.0	Cytek	
Prism 9.4.1	GraphPad	
Biorender	Biorender.com	
Cell Ranger ARC v2.0.0	10X Genomics	
Loupe Cell Browser	10X Genomics	
Morpheus	Broad Institute	
FCS Express 7 Research Edition v7.14.0020	De Novo Software	
FACSDiva v9.0	BD Biosciences	
Other		
gentleMACS C-tube	Miltenyi Biotec	130096334
gentleMACS Dissociator	Miltenyi Biotec	130-093-235
Passive Avoidance Chamber and Shock Control	Maze Engineers	
Hot Plate	Maze Engineers	
Control Company 3389 Variable Speed Peristaltic Tubing Pump	Mitchell Instrument Co	CNC-3389
Cytek Aurora	Cytek	
Illumina NextSeq 2000	Illumina	
2100 Bioanalyzer	Agilent	
Synergy HTX	Agilent	BTS1LFTA
Seahorse XFe24 Analyzer	Agilent	
405TS Microplate Washer	Agilent	Cat# 405TS

Bio-Plex 200 System with HTF	Bio-Rad	#171-000205
Bio-Plex Pro™ Wash Station	Bio-Rad	#30-034376
CFX Connect Real-Time PCR Detection System	Bio-Rad	Cat# 1855201
iMark Microplate reader	Bio-Rad	Cat #1681135
LSRFortessa Flow Cytometer	BD Biosciences	